

UC San Diego

UC San Diego Previously Published Works

Title

Paleointensity determination from São Miguel (Azores Archipelago) over the last 3 ka

Permalink

<https://escholarship.org/uc/item/4w93j9gk>

Journal

Physics of the Earth and Planetary Interiors, 234

Authors

Di Chiara, Anita
Tauxe, Lisa
Speranza, Fabio

Publication Date

2014-09-01

Peer reviewed

Manuscript Number: PEPI-D-14-00015

Title: Paleointensity determination from São Miguel (Azores Archipelago) over the last 3 ka

Article Type: Research Paper

Keywords: Paleomagnetism; paleointensity; Azores; Atlantic Ocean; global spike

Corresponding Author: Dr. ANITA DI CHIARA,

Corresponding Author's Institution: USP

First Author: ANITA DI CHIARA

Order of Authors: ANITA DI CHIARA; Lisa Tauxe, Prof.; Fabio Speranza, Dr.

Abstract: Paleointensity data from the Atlantic Ocean are rare. We present new paleointensity data from São Miguel (Azores Islands, Portugal) based on 20 paleomagnetic sites from 13 lava flows emplaced over the last 3,000 years. Ten lava flows are radiocarbon dated (Moore 1990, 1991; Moore and Rubin, 1991), whereas three flows were archeomagnetically dated by Di Chiara et al. (2012) and one site was dated using stratigraphic relations. All the samples, previously investigated to recover paleodirections (Di Chiara et al., 2012), were subjected to IZZI experiments. Importantly, the new data are internally consistent, agree with Moroccan, and European datasets, and offer new constraints for CALS style models (e.g., Korte and Constable 2011). The inferred Virtual Axial Dipole Moments (VADMs) range from 68.2 ZAm² and 163.5 ZAm². A peak in field strength with an estimated age of around 600 BCE is well supported by two sites from the same flow (Furna), and is comparable to the "spike" of intensity found in Portugal of the same age (Nachasova et al., 2009) and at about 1000 BCE in the Levant (Ben-Yosef et al., 2009; Shaar et al., 2011). A gradient in VADM values with latitude observed by Mitra et al. (2013) between 100 to 1000 AD is confirmed as well as its absence from between 0 to 100 AD.

Anita Di Chiara

Tel.: +55 11 950594087

e-mail: dichiaranita@gmail.com

February 11th, 2014

PEPI
Editor-in-chief

Dear Sir,

I am sending you the electronic version of the paper “Paleointensity determination from São Miguel (Azores Archipelago) over the last 3 ka”, by Anita Di Chiara, Lisa Tauxe and Fabio Speranza, that I would like to submit to *Physics of the Earth and Planetary Interiors*.

No part of this paper has been published or submitted elsewhere.

As possible reviewers, I suggest paleomagnetist who are well known for their solid experience on the study of the paleointensity of the geomagnetic field:

Dr. Monika Korte,
Helmholtz Centre Potsdam
GFZ German Research Centre for Geosciences
Behlertstraße 3a Building K 3, room 116
14467 Potsdam (Germany)
e-mail: monika.korte@gfz-potsdam.de

Dr. Miriam Gòmez Paccard
Géosciences Rennes
Campus Beaulieu, Université de Rennes 1
35042 Renne, France
e-mail: miriam.gomez@univ-rennes1.fr

Dr. Yongjae Yu,
Department of Geology and Earth Environmental Sciences,
Chungnam National University, Daejeon, South Korea
e-mail: yongjaeyu@cnu.ac.kr

Yours sincerely,

Anita Di Chiara (on behalf of the co-authors)

1 Paleointensity determination from São Miguel (Azores Archipelago) over
2 the last 3 ka

3 Anita Di Chiara*^{1,2,3}, Lisa Tauxe⁴, and Fabio Speranza¹

4 ¹ *Istituto Nazionale di Geofisica e Vulcanologia, via di Vigna Murata 605, Roma, Italy,*
5 *dichiaraanita@gmail.com, fabio.speranza@ingv.it*

6 ² *University of Bologna, Bologna, Italy*

7 ³ *Universidade de São Paulo, IAG, Rua do Matão 1226, SP, Brasil*

8 ⁴ *Geosciences Research Division, Scripps Institution of Oceanography, 8622 Kennel*
9 *Way, La Jolla, CA, United States, ltauxe@ucsd.edu*

10
11 **Abstract**

12 Paleointensity data from the Atlantic Ocean are rare. We present new paleointensity
13 data from São Miguel (Azores Islands, Portugal) based on 20 paleomagnetic sites from 13
14 lava flows emplaced over the last 3,000 years. Ten lava flows are radiocarbon dated (Moore
15 1990, 1991; Moore and Rubin, 1991), whereas three flows were archeomagnetically dated by
16 Di Chiara et al. (2012) and one site was dated using stratigraphic relations. All the samples,
17 previously investigated to recover paleodirections (Di Chiara et al., 2012), were subjected to
18 IZZI experiments. Importantly, the new data are internally consistent, agree with Moroccan,
19 and European datasets, and offer new constraints for CALS style models (e.g., Korte and
20 Constable 2011). The inferred Virtual Axial Dipole Moments (VADM) range from 68.2
21 ZAm^2 and 163.5 ZAm^2 . A peak in field strength with an estimated age of around 600 BCE is
22 well supported by two sites from the same flow (Furna), and is comparable to the “spike” of
23 intensity found in Portugal of the same age (Nachasova et al., 2009) and at about 1000 BCE
24 in the Levant (Ben-Yosef et al., 2009; Shaar et al., 2011). A gradient in VADM values with
25 latitude observed by Mitra et al. (2013) between 100 to 1000 AD is confirmed as well as its
26 absence from between 0 to 100 AD.

27 **Highlights**

28 1. New paleointensity data from 24 dated sites from São Miguel (Azores) of the last 3
29 ka

30 2. Data will provide new constraints for global models

31 3. High intensity around 600 BC suggests a regional or global spike.

32 4. We confirm the latitudinal gradient in VADM seen between Western Europe and NW
33 Africa

34 Key words: Paleomagnetism; paleointensity; Azores; Atlantic Ocean; global spike

35 **1. Introduction**

36 The modern geomagnetic field is dominated by a geocentric axial dipole but there are
37 significant departures from the simple bar magnet model. These manifest themselves as large
38 patches of anomalous behavior, known as “flux patches”. There are currently two of these
39 positive anomalies in the northern hemisphere, one over Eurasia and one over North America
40 (lower inset to Figure 1).

41 Direct measurement of intensities began in 1840 AD (when C. F. Gauss devised the first
42 method to measure it), whereas measurement of directions (declination and/or inclination) are
43 available since before 1600 AD. Jackson et al. (2000) combined the global model directions
44 with a linear extrapolation of paleomagnetic intensity measurements to estimate the strength
45 of the magnetic field over the period since 1600 AD, and produced a time dependent spherical
46 harmonic field model for that time period (GUFM). To understand the longer term behavior
47 of the geomagnetic field, we rely on paleo and archeomagnetic studies.

48 The GEOMAGIA database was created by Donadini et al. (2006), then expanded
49 (Donadini et al., 2009) and is updated periodically; it contains archeointensity, and
50 paleointensity data from volcanics, as well as directions. The temporal and geographical
51 distribution of data is uneven. For the last 10 kyr, a large amount of data has been published
52 from continents with the majority coming from Europe. While there have been several recent
53 studies as far west as Portugal (Nachasova and Burakov , 2009, Hartmann et al., 2009), and
54 Morocco (Kovacheva 1984, Gómez Pacard et al., 2012), the central-northern Atlantic Ocean
55 is, apart from historical (Michalk et al., 2008) and post-glacial lavas from Iceland (Schweitzer
56 and Soffel, 1980; Stanton et al., 2011; Tanaka et al., 2012), is essentially devoid of data.
57 Consequently, global models (e.g., CALSxk.x family and ARCH3k) have very few
58 constraints from the central northern Atlantic (Korte et al., 2009; Donadini et al., 2009; Korte
59 and Constable, 2011; Genevey et al., 2008).

60 In contrast, there is a robust and rapidly growing data set for Europe. Particular features
61 in the secular variation models, likely representing the growth and decay of flux patches are
62 well constrained and reproduced by several different studies from different regions. Between
63 2500-3000 years ago, a rapid change in intensity was recorded in Europe (Gallet and Le Goff,
64 2006; Ben-Yosef et al., 2008a; Genevey et al., 2009), reaching the highest values in the
65 Southern Levant area (Ben-Yosef et al., 2009) of up to 213.1 ZAm^2 between $816 \pm 17 \text{ BCE}$
66 and $983 \pm 25 \text{ BCE}$. Recently, data from the Balkan area ($80 \mu\text{T}$, or 173.3 ZAm^2 dated at around
67 500 BCE; Tema and Kondopoulou, 2011) confirm the high value, whereas data from Italy
68 (Tema et al., 2013) are too scattered to confirm the possible spike. High field values for the
69 same period were obtained from the Western US (Champion, 1980; Hagstrum and Champion,
70 2002) (values up to 140 ZAm^2), and even higher values of up to 200 ZAm^2 from Hawaii
71 (Pressling et al., 2006) (although these were not reproduced in the later studies of Pressling et
72 al., 2009). And recently, values of around 130 ZAm^2 were observed at about 1320-1380 BCE
73 in Korea by Hong et al. (2013). These data suggest the possibility of a high dipolar field at
74 that time, and encourage further investigations of the regional extent of this feature (or these
75 features). Our data serve to explore this hypothesis.

76 The Azores Archipelago is an ideal location for gathering new paleointensity data, as
77 historical and pre-historical lava flows are well exposed and geochronologically dated (e.g.,
78 Feraud et al., 1980; Moore 1990, 1991; Moore and Rubin, 1991). A paleosecular variation
79 curve (PSV) was obtained based on 16 lava flows emplaced over the last 3 kyr on Sao Miguel
80 (Di Chiara et al. 2012). The PSV curve was reconstructed using 27 radiocarbon dated sites
81 from 16 lava flows, together with 6 directions gathered by Johnson et al. (1998). Sister
82 specimens from the same samples from sites investigated by Di Chiara et al. (2012) were
83 analyzed in this study, in order to obtain new paleointensity data.

84 **2. Geological setting and studied lava flow deposits**

85 São Miguel is the largest (760 km^2) of the nine volcanic islands of the Azores
86 Archipelago, straddling the Mid Atlantic Ridge at the triple junction of the North American,
87 Eurasian and African plates (Fig. 1). Four large trachytic stratovolcanos developed from 8.1
88 Ma (Abdel-Monem et al., 1975; Feraud, et al., 1980) to historical times. From east to west, six
89 volcano-stratigraphic units had been recognized: Nordeste, Furna, the plateau do Congro,
90 Agua de Pau, Região dos Picos, and Sete Cidades Volcano. The “Waist Zone” (Booth et al.,
91 1978), or “Zone 2”, or “Região dos Picos” (Moore, 1990, 1991), is the most populated area
92 of the island. The Região dos Picos is a flat area of basaltic lava flows speckled with volcanic

93 cones. Two historical eruptions occurred on the island, both located in the central part and the
94 eastern part of the Região dos Picos. The Fogo eruption in 1563 AD was the most recent high
95 explosive (subplinian) eruption at Fogo (subplinian) inland and at Fogo caldera. It also
96 produced two thin lava flows originating from the monogenetic Queimado cone, nearby to the
97 Ponta das Praias locality (f5b in Fig.1). The other historical eruption was the most recent
98 inland effusive eruption which was emplaced from the Fogo 1 cone in 1652 AD (unit f9b on
99 Fig. 1). This flow reached both the northern coast (at Rabo de Peixe town) and the southern
100 coast nearby to the town of Lagoa. The two historical flows are described in chronicles by
101 Mitchell-Thomè (1981) and Booth et al., (1978). For older flows, boundaries were delimited
102 on the geological map of Moore (1990) based on field evidence. Satellite images were of little
103 use as only small scoria cones dotting the area are evident and the lava flow limits are covered
104 by vegetation and by human colonization.

105 We sampled these two historical lava flows in July 2010, as well as an additional 32
106 paleomagnetic sites, with at least 15 well-spaced cores at every site. Cores were oriented both
107 by solar and magnetic compass. In all, we sampled 16 flows at 35 sites as described in Di
108 Chiara et al., (2012) (Fig. 1 and Table 1 in Di Chiara et al., 2012). These span an age range
109 between 3 ka and 1652 AD. Seven sites from some of the same flows were also investigated
110 paleomagnetically by Johnson et al. (1998). Combining the two studies, 31 sites yielded
111 reliable paleomagnetic results. All the pre-historical radiocarbon ages reported by Moore
112 (1990, 1991) and Moore and Rubin (1991) were recalibrated by us with the Stuiver's Online
113 program Calib6.0 (Stuiver et al., 2009). An additional four of the 16 sampled flows were
114 dated using the comparison of the paleomagnetic directions (see Table 2 in Di Chiara et al.,
115 2012): Cruz N and S, Lagoa, and Caloura flows (marked in Table 1) with recalculated
116 reference curves. Recently, it was suggested that paleointensity estimates could be used in
117 conjunction with geomagnetic global field models (e.g., Jackson et al., 2000; Korte and
118 Constable, 2011), to help constrain eruptive ages for young lavas (Carlut and Kent, 2000; Gee
119 et al., 2000; Carlut et al., 2004; Bowles et al., 2005). We explore the latter in Section 4.2.

120 **3. Methods**

121 To achieve our purpose, we first tackled the methodological issue of what is the optimal
122 method by which to recover the paleointensity of the Earth's magnetic field. Indeed, over the
123 past forty years a large number of techniques have been proposed to improve the quality and
124 reduce the time of experiments for absolute paleointensity (e.g., Coe et al., 1978; Shaw, 1974;
125 Hoffman et al., 1989; Tauxe and Staudigel, 2004; Dekkers and Böhnell, 2006; see review by

126 Tauxe and Yamazaki, 2007). Despite (or because) of these efforts, there remains no consensus
127 on the best method. Therefore, some procedures remain controversial and poorly tested.

128 By far, the Thellier family of experiments (e.g., Thellier and Thellier, 1959) is the most
129 accepted and widely used method to recover paleointensities. It is based on two main
130 assumptions: 1) a linear relationship exists between the geomagnetic field and the thermal
131 remanent magnetization (TRM); 2) during the experiments no alteration of the ability to
132 acquire thermal remanence occurs and normalization of the natural remanent magnetization
133 (NRM) with a laboratory TRM yields an accurate estimate for ancient field strength. The first
134 assumption has been verified for single domain materials, but frequently fails for multi-
135 domain remanences. Given these constraints, suitable materials are rare: we require an
136 original component of NRM, carried by single domain ferromagnetic minerals, with no
137 evidence of alteration during laboratory analysis. Therefore, one of the best approaches for
138 testing the validity of the absolute paleointensity determination is to deal with quickly cooled
139 lava flow deposits (e.g. Pan et al., 2002) and basaltic glasses (Pick and Tauxe, 1994; Ferk et
140 al., 2008; Cromwell et al., 2011). Many cross-tests of the different techniques on historical
141 flows of measured intensity have been carried out in order to assess various techniques and to
142 identify the best method. For instance, at least nine studies have focused on the 1960 lava
143 flow from the Big Island of Hawaii (Abokodair, 1977; Tanaka and Kono, 1991; Tsunakawa
144 and Shaw, 1994; Tanaka et al., 1995; McClelland and Briden, 1996; Valet and Herrero-
145 Bervera, 2000; Hill and Shaw, 2000; Yamamoto et al., 2003; Herrero-Bervera and Valet,
146 2009); these studies are marked by their inability to recover the ancient magnetic field
147 accurately. More recently however, Cromwell et al. (2012) have achieved an unprecedented
148 accuracy in recovering the historical field from the 1960 and other historical lava flows by
149 sampling the finest grained (glassy) portions of the flow and using the IZZI method of Tauxe
150 and Staudigel (2004). We therefore use the IZZI protocol in this study.

151 The IZZI protocol is a combination of two versions of the original method, one
152 proposed by Aitken (1988; in-field, zero-field; IZ) and one by Coe (1967; zero-field, in-field;
153 ZI), thus it alternates the IZ and ZI steps, and adds a pTRM check step after every ZI step.
154 The advantages of this technique are triple: 1) the angular dependence between the Natural
155 Remanent Magnetization (NRM) and the Thermal Remanent Magnetization acquired during
156 experiments under a known laboratory field (TRM_{lab}) can be easily detected, indicated as an
157 angle θ ; 2) it provides a quantitative estimate for the consistency of the outcome between IZ
158 and ZI steps thereby allowing detection of so-called pTRM tails that bias paleointensity

159 results; 3) it is quicker because the “pTRM tail check” of Riisager and Riisager (2001) is
160 unnecessary.

161 Results are classically displayed and analyzed through the Arai plot (Nagata et al.,
162 1963), a scatter plot displaying residual NRM (‘NRM remaining’) versus cumulative
163 pTRMs. If the material fulfills the assumptions underlying the Thellier method (i.e. the NRM
164 is a pure TRM carried exclusively by stable SD), then the Arai plot is a straight line,
165 connecting the two (x, y) endpoints: (0, NRM), and (TRM, 0). The most common approach to
166 calculating the true intensity of the paleomagnetic field is the best-fit line. Some authors tend
167 to use only the low-temperature slope while others argue that the low-temperature slope can
168 significantly overestimate the true field (e.g. Biggin and Thomas, 2003; Calvo et al., 2002;
169 Chauvin et al., 2005). Some authors suggest averaging the slope of the two segments (e.g. Hill
170 and Shaw, 2000), and others recommend using as large a segment as possible even if it is
171 curved (e.g. Levi, 1977; Biggin and Thomas, 2003; Chauvin et al., 2005). An alternative
172 option is using only the two end-points of the Arai plots when specimens show little signs of
173 alteration (e.g. Coe et al., 2004; Garcia et al., 2006).

174 The difficulty of interpretation arises from the multiple causes of failure that can affect
175 results, causing a shift from an ideal straight line: i) multi-domain (MD) grains can cause
176 concave, or convex, or ‘S-shaped’ curves (see Levi 1977; Xu and Dunlop, 1995, 2004; Biggin
177 and Thomas, 2003; Coe et al., 2004; Fabian, 2001; Leonhardt et al., 2004) in the Arai Plot;
178 and ii) the difference of direction between the NRM with respect to the laboratory field
179 applied during Thellier experiments (Xu and Dunlop, 2004; Fabian, 2001, Leonhardt et al.,
180 2004; Biggin 2006; 2010; Biggin and Poidras, 2006; Shaar et al., 2011), expressed as an angle
181 θ , which likely is responsible for the zig-zagged behavior (when the NRM is perpendicular to
182 the laboratory field the deviation is high).

183 Zigzags are unique features of the IZZI protocol (Tauxe and Staudigel, 2004; Yu et al.,
184 2004; Yu and Tauxe, 2005; Shaar et al., 2011), and they occur when the IZ and the ZI data
185 points create two distinct curves. Several attempts to quantify the zigzagging have been
186 proposed (e.g. Granot et al., 2006; Tauxe, 2009). Following these findings, Shaar et al.,
187 (2011) performed experiments to demonstrate that experimental conditions can influence
188 paleointensity experiments. In particular, factors that play an important role are the difference
189 of the intensity of the field laboratory (B_{TRM}), and the original NRM of the sample (B_{NRM}),
190 and the angle between B_{TRM} and B_{NRM} (θ). Linear curves can occur when $\theta = 0^\circ$ and
191 $B_{\text{TRM}}/B_{\text{NRM}} = 1$, and semi-linear curves with a weak zigzag occur when $\theta = 0^\circ$ and $B_{\text{TRM}}/B_{\text{NRM}}$

192 ≤ 2 . Concave curves occur when $\theta = 180^\circ$, regardless the ratio $B_{\text{TRM}}/B_{\text{NRM}}$. Convex curves
193 occur when $\theta = 0^\circ$ and $B_{\text{TRM}}/B_{\text{NRM}} = 4$. The two endpoints of a non-linear plot (concave or
194 convex) connected together yields the ideal SD line. For the same $B_{\text{TRM}}/B_{\text{NRM}}$ the zigzag is
195 weak for $\theta = 0^\circ$ and strong for $\theta = 180^\circ$. Convex curves in the Arai plots result when the field
196 in the paleointensity oven is stronger than the ancient field. Shaar et al. (2011) defined a new
197 parameter, the “IZZ_I_MD”, which calculates the total area bounded by the IZ and the ZI
198 curves normalized by the length of the ZI curve, and stating that the degree of zigzag
199 increases with $B_{\text{TRM}}/B_{\text{NRM}}$ and as θ deviates from 90° toward 0° or 180° . These effects are
200 thought to be responsible for an underestimation or overestimation of the paleointensity.

201 As a result of experimental complications, a key problem is to adequately choose the
202 criteria by which individual results are selected or rejected. Again there is little consensus
203 (e.g. Biggin and Thomas, 2003; Kissel and Laj, 2004; Selkin and Tauxe, 2000; Tauxe, 2009;
204 Shaar and Tauxe, 2013) and cut-off values of the selection statistics vary greatly among
205 various studies.

206 Here, we test various suggestions for enhancing the IZZI method (by Tauxe and
207 Staudigel, 2004; Valet et al., 2010; Shaar et al., 2011; and Tanaka et al., 2012). We hoped to
208 carefully screen all the samples in a preliminary step and reject all that do not fulfill the
209 assumptions underlying the technique (a single-component TRM carried by SD magnetic
210 particles that do not alter during experiments). Thus, all the samples that do not fulfill the
211 assumptions underlying the technique and diverge from an ideal behavior of a single-
212 component of TRM, carried by SD magnetic particles that do not alter during experiments,
213 were excluded from paleointensity experiments (as suggested by Valet et al., 2010). The aim
214 is to minimize the source of bias affecting the success of paleointensity results, for example
215 samples that displayed evidence of multi-component NRM. Hence, we selected those samples
216 (1) with no evidence of secondary remagnetizations, (i.e, those with a Zijderveld diagram
217 trending straight to the origin), (2) displaying “square-shouldered” blocking temperature
218 spectra (thought to minimize the presence of MD grains), and (3) displaying reversible
219 features on the susceptibility-temperature curves (previously obtained from all the samples),
220 as well as those revealing a single Curie Temperature. Indeed, as particle size increases
221 (Carlut and Kent, 2000) and MD grains are a predominant carrier of the remanent
222 magnetization (Levi, 1977; Fabian 2001; Riisager and Riisager 2001; Leonardht et al., 2004)
223 the Arai plots tend to have a non-linear behavior, and cause the failure of the experiments.
224 Using these guidelines, all the samples previously thermally-treated to recover paleomagnetic

225 directions (Di Chiara et al., 2012) were screened and samples displaying non-ideal behavior
226 were rejected from any further analysis.

227 From the 390 samples from 33 sites that yielded reliable paleodirections after the
228 thermal demagnetization cleaning analyses (Di Chiara et al., 2012), only 64 samples from 28
229 sites passed the first rigorous pre-selection step, and were subjected to paleointensity
230 experiments. From each sample, 2 to 6 fresh sister specimens were chosen and a total of 180
231 specimens were prepared for the paleointensity experiments. Individual chips were placed in
232 clean glass vials and fixed into position with microfiber glass filters and Kasil “glue”. The
233 paleointensity experiments were carried out using the in-field, zero-field, zero-field, in-field
234 (IZZI) protocol (Tauxe and Staudigel, 2004). We did not include a “pTRM tail check” step as
235 it is redundant and unnecessarily adds to the number of heating steps. The protocol was
236 carried out as follows: specimens placed in the glass vials were heated to 100°C and cooled in
237 zero field (zero-field step); after measuring the remaining NRM, specimens were reheated to
238 100°C and cooled in laboratory field, directed along the Z axis and re-measured (In field
239 step). The difference between the first NRM and the second step is the partial TRM (pTRM)
240 gained by cooling from 100°C to room temperature. At each subsequent temperature step, the
241 order of the double heating procedure was reversed such that specimens were cooled in-field
242 (I) first, then in zero-field (Z) (Zero-field/In-field, ZI, and In-field/Zero-field, IZ). The so-
243 called pTRM check step consists of going back to the previous heating step and repeating the
244 in-field heating in order to check if the ability of the specimen to acquire pTRM changed
245 during the intervening heating steps. The procedure consists of a total of 43 heating steps
246 alternating IZ and ZI and the pTRM checks, in 100 °C interval up to 300 °C, 50 °C up to
247 500°C and 10°C up to 600°C. All the experiments were performed in the shielded room of the
248 paleomagnetic laboratory of The Scripps Institution of Oceanography (La Jolla, California,
249 US) using double shielded water-cooled ovens for paleointensities and the 2G cryogenic
250 magnetometer.

251 In order to test whether the orientation of the NRM parallel to the laboratory field
252 affects the robustness of the results (as suggested by Fabian, 2001; Leonhardt et al., 2004; Xu
253 and Dunlop, 2004; Yu et al., 2004; Biggin, 2006; 2010; Biggin and Poidras, 2006; Shaar et
254 al., 2011a) two separate types of experiments were performed. In one type, a total of 90 sister
255 specimens were oriented by placing them in vials, with their NRM directions quasi parallel to
256 the applied field direction, thus with a specimen remanent inclination between -70° and -89°

257 (that is parallel to z-axis of the 2G cryogenic Magnetometer). The remaining 90 specimens
258 were randomly oriented with respect to the laboratory field.

259 Many authors stressed the importance of choosing a laboratory field equal to or slightly
260 lower than the expected paleofield (e.g., Shaar et al., 2011; Paterson et al., 2012). The
261 expected value of the field (Korte et al., 2011) averaged for the different ages of our samples
262 is about 40 μ T, so we chose 40 μ T as the laboratory field.

263 In addition to the paleointensity experiments, we also carried out routine magnetic
264 analyses on 30 specimens (about one per site) to characterize the magnetic mineralogy.
265 Hysteresis properties were measured using a Princeton Measurement Corporation MicroMag
266 alternating gradient magnetometer (AGM, model 2900) with a maximum applied field of 1 T.
267 The measured hysteresis parameters include saturation magnetization (M_s), saturation
268 remanent magnetization (M_{rs}), coercive force (B_c) and the coercive force of the remanence
269 (B_{cr}). The ratios between M_r/M_s and B_{cr}/B_c were plotted in a Day diagram (Day et al.,
270 1977).

271

272 **4. Results**

273 **4.1 Magnetic mineralogy**

274 In Figure 2 we plot hysteresis ratios of saturation remanence to saturation magnetization (M_r/M_s)
275 and coercivity of remanence to coercivity (B_{cr}/B_c) for the Azores sample collection as blue
276 squares. The M_r/M_s versus B_{cr}/B_c data plot in a swath well displaced from the linear SD-MD
277 mixing curve (e.g., Dunlop 2002; Dunlop and Carter-Stiglitz, 2006) shown as the solid red line. The
278 theoretical curve is calculated using the SD and MD end-members from CS912 and 041183 in
279 Dunlop and Carter-Stiglitz (2006) respectively in the equations suggested by Dunlop (2002). Our
280 data do not follow the theoretical curve for SD-MD mixing; instead, the data are quite similar to
281 those measured on submarine basaltic glasses by Tauxe et al. (1996), modeled as mixtures of multi-
282 axial SD and superparamagnetic (SP) particles (Tauxe et al., 2002).

283 We show hysteresis loops for three representative flows (Mos: Sml1507b, Furna:
284 Sml2614a and Feteiras: Sml0511b) in Figures 3a-c. Figure 3a is characteristic of single
285 domain (SD) magnetic assemblages or nearly so, with a M_r/M_s ratio of 0.47. The behavior
286 shown in Figure 3b is not pure SD but appears to be slightly ‘wasp-waisted’, indicating a

287 mixture of SD and SP (Pick and Tauxe, 1994). Figure 3c is ambiguous, and could be an
288 assemblage of so-called ‘pseudo-single domain’ (PSD) grain sizes with vortex structures in
289 their remanent state, or nearly multidomain (MD) assemblages. Figures 3d-f show
290 representative stepwise thermal demagnetization curves for sister specimens from the same
291 flows as those shown in Figures 3a-c. In the first two demagnetization curves (Figures 3d and
292 3e), the fractional magnetization drops over a narrow range of temperatures, close to the Curie
293 point, displaying a coherent trend among all specimens from the same flow. Thus between 60-
294 80% of the remanence unblocks above temperatures of 400-500°C, consistent with the
295 suggestion of dominantly single domain behavior from the hysteresis loop shown in Figure
296 3a. Figure 3e drops in a slightly more gradual fashion than Figure 3d. Figure 3f shows at least
297 one specimen that demagnetizes over a more distributed range of blocking temperatures.
298 Lower blocking temperatures can be the result of grains near the SP/SD threshold size, or
299 could result from PSD grains. Based on the behavior during the paleointensity experiments
300 discussed in the following, we suggest that the slightly wasp-waisted loop, coupled with
301 slightly lower blocking temperatures shown in Figures 3b and 3h reflect a grain size
302 distribution that spans the SP/SD range, and the behavior shown in Figures 3c and 3f results
303 from a distribution including larger PSD grains.

304 The behavior of specimens during the paleointensity experiment associated with the
305 three styles of hysteresis loops is illustrated in the bottom panel of Figure 3 (Figures 3g, h, i).
306 In the case in which the hysteresis behavior is close to an ideal SD assemblage, and the
307 blocking temperature spectra drops near the Curie point of magnetite (Figures 3a,d) the
308 specimens behave very well during the paleointensity experiment (Figure 3g). On the
309 contrary, the hysteresis behavior shown in Fig. 3c, which may reflect coarser grain sizes is
310 associated with less than ideal behavior during the paleointensity experiment (Fig. 3f, i).

311 We find that when magnetic mineralogy reveals the presence of SD grains as main
312 carrier of remanent magnetization, paleointensity results are usually reliable. Where PSD and
313 MD grains are main carrier of remanent magnetization, the paleointensity results are generally
314 less ideal. Nonetheless, magnetic mineralogy from different sites sampled from the same
315 flow, as well as different samples collected from the same site, display different mineralogical
316 characteristics. Thus, we conclude that while mineralogical analyses might be useful for
317 predicting which specimens will behave well during the paleointensity experiments (as
318 suggested by Valet et al., 2010), specimens from the same sample and samples from the same

319 flows show different (magnetic) behaviors and the paleointensity experiment itself must
320 provide the information necessary for accepting and rejecting specimen interpretations.

321

322 **4.2 Paleointensity results**

323 The results of the experiment are presented and analyzed through the ‘Arai plot’
324 (Nagata et al., 1963) in Figures 3g-i and Figure S1. We used the MagIC.py program (version
325 pmagpy-2.214, <http://earthref.org/PmagPy/cookbook>) to process and display results of
326 experiments. The results exhibit a variety of behaviors in the Arai plots. Three types of shapes
327 have been observed in the Arai plots: the 13.8% have a segmented or concave shapes (Figs.
328 3i, S1 a, d), the 8.3% have a zig-zagged character (Figs. 3i, S1 h, i), and the remaining 77.9%
329 exhibit straight or nearly straight lines (Figs. 3g, h and S1 b, c, e). Acceptable paleointensity
330 estimates have a linear Arai diagram, but specimens with nearly ideal behavior can depart
331 slightly from linearity. The acceptability limits are still a matter of discussion. Despite the
332 plethora of statistics to quantify the quality of the data, the selection of data remains
333 subjective. To ensure the reliability of our interpretations, we have chosen rather strict
334 selection criteria (see Tauxe, 2010 and Shaar and Tauxe, 2012 for definitions), which are
335 listed in Table 2. For specimens passing our selection criteria, the absolute value of the slope
336 of the best-fit line (green lines in the diagrams) multiplied by the laboratory field yields the
337 intensity of the ancient field. Specimens meeting our criteria (108 of 180) are listed in
338 Supplementary 2, representing a success rate of 60 % at the specimen level.

339 As suspected from phenomenological models and previous experimental results (e.g.,
340 Yu et al., 2004; Shaar et al., 2011), we confirm that the orientation of B_{TRM} and B_{NRM} can
341 influence the degree of zig-zag (S1), which tends to disappear when B_{TRM} and B_{NRM} directions
342 are nearly parallel. That said, when PSD or MD grains dominate, the behavior during the
343 paleointensity experiment produces erratic or curved Arai plots and experiments fail,
344 regardless of orientation. We suggest therefore that the effort of orienting specimens with
345 respect to the laboratory field is not worthwhile, while pre-selecting specimens using their
346 behavior during thermal demagnetization of the NRM (as suggested by Valet et al. (2010)
347 may be (although variability among samples and specimens makes even this problematic). We
348 find that those samples which show a rapid decrease of at least ~~the~~ 70% of the initial
349 magnetization over a narrow range of temperatures (close to Curie point), appear to perform
350 better. Hysteresis statistics do not help during preselection, as there is no clear relation

351 between the success of the experiments, most likely due to the non-uniqueness of hysteresis
352 ratios in detecting domain state. Despite the carefulness in the pre-selection of suitable
353 specimens, however, many specimens (~40%) still failed our selection criteria.

354 Specimens are taken as independent estimates of the field and are averaged at the lava
355 flow level (Table 3). For this study we consider a site to be acceptable if ~~it~~ at least 3
356 specimens and a standard deviation of at most 15 % or 5 μT (Table 2). Nine sites failed as no
357 reliable sample interpretations were found (Sml07, 10, 11, 16, 22, 24, 25, 30 and 33). The site
358 level consistencies of the remaining sites (as indicated by σ) are between 0.9 and 11.6 (with
359 an average of 4.7) or between 1.9% and 14.3%. Paleointensity values range between ~38 μT
360 (Queimado flow) and ~92 μT (Furna flow, radiocarbon dated to 593 ± 236 BC). Importantly, in
361 most cases, sites from flows that are similar in age (e.g., Cascalho ~1300 AD, Ponta da
362 Ferraria 1209 ± 54 AD, and Feteiras 1073 ± 90 AD) share similar paleointensity values (53.1
363 μT , 63.0 μT and 53.5 μT respectively). The two sites from the 1563 Queimado flow (Sml 19
364 and Sml 34) agree well with one another (Table 2) and also with Sml 31 which was thought to
365 represent the same eruption based on similarity in directions (Di Chiara et al., 2012). These
366 three flows have been averaged together in Table 3.

367 5. Discussion

368 Figure 4 is a summary of all directional (Di Chiara et al., 2012) and intensity (this
369 study) results from the Azores as well as the vector components predicted for São Miguel
370 (37.8°N , 25.5°W) by the ~~most recent~~ global field model, ~~the~~ Cals3k.4 by Korte and Constable
371 (2011), the French archeomagnetic curve (Bucur, 1994; Gallet et al., 2002) and the
372 ARCH3k.1 model of Korte et al. (2009). Our mean-paleointensity data vary from 38.5 ± 4.3 μT
373 (Queimado flow) to 92.3 ± 11.6 μT (Furna flow). At first glance, our results agree with the
374 global model predictions fairly well. Indeed, the maximum discrepancy between mean
375 intensities and predictions from the Queimado flow (1563 AD), Feteiras (1073 ± 90 AD), Mata
376 das Feiticeiras (1048 ± 113 AD), Caldeirão (675 ± 107 AD) and Ponta das Praias (240 ± 168 AD)
377 flows is 9 μT . Considering that the models are highly smoothed, the agreement is very good.
378 However, the intensities from Furna, Caldeirão, Fogo and Lagoa are quite different from the
379 expected values.

380 Ten of the studied flows are radiocarbon dated by Moore (1990) and Moore and Rubin
381 (1991). Three lava flows had been paleomagnetically dated by Di Chiara et al. (2012): Cruz N
382 (29; 400-700 BC), Cruz S (11; 0-200 AD), and Lagoa (14; 100-400 AD). Unfortunately, Cruz

383 S did not pass our selection criteria. ~~While~~ Cruz N agrees with the predicted intensity value,
384 the intensity from Lagoa deviates from the expected values by about 15 μT . We suggest that
385 either the field was lower than predicted by the global model, or paleomagnetic directions in
386 some cases are not sufficient for dating and the inferred ages of the site was erroneously
387 assigned. Stressing that there were few data points in the Atlantic Ocean region to constrain
388 the global model, we nonetheless observe that predicted directional values agree reasonably
389 well with the data of Di Chiara et al., (2012), particularly the ARCH3k model. Additionally,
390 the direction of the Ponta das Praias flow (Sml28, ~240 AD), is in good agreement with the
391 models, and has an intensity significantly higher than the Lagoa site. Thus, we suggest that
392 the ages of Lagoa dated using paleomagnetic directions were erroneously assigned.

393 Considering paleodirection (Declination, D, and Inclination, I, Table 2) and
394 paleointensity values and comparing them with the Cals3k.4 (from 0 to 3 ka), Cals10k (from
395 3 to 10 ka, by Korte et al., 2011), and ARCH3k.1 (from 0 to 3 ka), we find that the Lagoa
396 flow is not uniquely dated by the field models. Effectively, the low values of declination
397 (1.0°), inclination (54.3°) and intensity ($44.9 \mu\text{T}$) of Lagoa flow are comparable with the
398 minimum reported in the Cals10k (Korte et al., 2011) in D, I and intensity (359.7° , 52.0° and
399 $40.8 \mu\text{T}$, respectively) around 3,100 BC. Another possibility is that the site Sml14 of the
400 Lagoa flow could even be historical, since it was sampled in a lava flow close to a branch of
401 the 1652 AD Fogo flow (according to the geological map of Moore 1990). This second
402 hypothesis cannot be discarded since the 1563 AD Queimado flow yielded similar values
403 ($D=0.5^\circ$, $I=55.5^\circ$ and intensity= $38.5 \mu\text{T}$).

404 The historical flow Fogo is characterized by an inclination (47.7°), which is discrepant
405 with respect to the global models (e.g., *gufm1* predicted an inclination of 63°), raising the
406 suspicion that either a rapid inclination drop occurred 150 years before the *gufm1* prediction
407 in the Atlantic area, or some problem in recording the paleomagnetic field occurred in the
408 flow, or the paleomagnetic sites were erroneously mapped as the Fogo flow but belong
409 instead to a slightly older flow. While the directions of Sml08 and Sml10 are consistent with
410 each other, we cannot test the intensities of Sml10 as it failed our selection criteria. Therefore
411 we suggest that Sml08 (named here Fogo1x) is somewhat older than reported, and both
412 direction and intensity suggest that it could have erupted at ~800 AD (similar to the Sml13).

413 The age of the Cascalho flow (Sml18) was constrained using stratigraphic evidence and
414 paleomagnetic directions. Indeed it was initially thought to fall in the 1300–1500 AD time

415 window. However, the inclinations are much lower than the Queimado flow of 1563 AD
416 (Sml19, 31 and 34) all of which are consistent with the model predictions. Therefore, we
417 reassign it to have an age within the lower bound of the interval (~1300 AD). The intensity of
418 $53.1 \pm 4.2 \mu\text{T}$ supports this hypothesis as the intensity agrees well with those obtained for the
419 1000-1300 AD age interval ($\sim 55 \mu\text{T}$), whereas it is significantly different from the values of
420 Queimado ($38.5 \pm 4.3 \mu\text{T}$).

421 Paleomagnetic directions from the Caldeirão flow (Sml17) agree well with global model
422 predictions, especially with the ARCH3k.1. The paleointensity of Sml23 (here named
423 Caldeirao E) is $10 \mu\text{T}$ lower than Sml17. The paleointensity of Sml24 (here named Caldeirão
424 W) is inconsistent with the model and could be older than 675 AD; instead a date of 593 ± 236
425 BC, the age of the Furna flow fits the model much better. The high intensity of Sml24, 100.6
426 μT , is indeed similar to the $89.4 \mu\text{T}$ of the Furna flow. Indeed, the map location of Sml24
427 could well be placed off the Caldeirão flow and in a window to an older flow.

428 **5.1 Paleointensities over the last 3 ka**

429 We have calculated mean values of paleomagnetic intensities and converted them to virtual
430 axial dipole moments (VADM, e.g. Tauxe, 2010). These are listed in Table 3 and plotted in
431 Figure 5; those with revised ages are indicated by the open, dashed symbols. We also show
432 data from Morocco (Gomez-Paccard et al., 2012), Portugal (Nachasova and Bukarov, 2009;
433 Hartmann et al., 2009; and Gomez-Paccard et al., 2012), Spain (Gomez-Paccard et al., 2006;
434 2008; 2012; Nachasova et al., 2007; Catanzariti et al., 2012; Beamud et al., 2012), and France
435 (Chauvin et al., 2000; Genevey and Gallet 2002; Gallet et al., 2003; 2009; Genevey et al.,
436 2009; Gomez-Paccard et al., 2012). The regional curve has two maxima (around 600-800 AD
437 and 600-400 BC, separated by a minimum at around 0-500 AD. The 600-400 BC maximum is
438 well reproduced by our Furna flow (593 ± 236 BC) reaching a high of $92.3 \mu\text{T}$ (163.5 ± 20.5
439 ZAm^2). This result is robust as it is based on an average of 17 specimens from two flows
440 (sampled 3 km far from each other) belonging to the same volcanic event. Similar high field
441 values around the same time interval are observed in the Western USA (Champion, 1980)
442 with values up to 140ZAm^2 , and even higher values of 197.5ZAm^2 from Hawaii (Pressling
443 et al., 2006) around 840 BC. The high value recovered on the Hawaiian samples was not
444 reproduced after a re-measurement of the samples however (Pressling et al., 2007). A regional
445 spike was also recorded in Europe (Genevey et al., 2003; Gallet et al., 2006; Gallet and Le
446 Goff, 2006), in Syria (Genevey et al., 2003) and in Southern Jordan (reaching as high as 213

447 ZAm², Ben-Yosef et al., 2008; 2009) at around 800 and 1000 BC respectively. However,
448 there is a discrepancy between the Levantine curve and the Grecian master curve (De Marco
449 et al., 2008), which highlights a peak of intensity of 114 ZAm² around ~600-500 BC.
450 Regardless of the age difference of the spike and the irregular distribution of datasets, both
451 European and Azorean data suggest the possibility of a large scale spike, and encourage
452 further investigation of the regional extent of this feature. Recent data from Eastern Asia by
453 Cai et al. (subm.) argue against the global nature of this spike because they do not find any
454 peak of intensity around ~1000 BCE in China, suggesting that the spike may not be global;
455 rather, the peaks in the Levantine and Southern European curves are distinct features of the
456 non-dipole field. Interestingly, the archeomagnetic data of Hong et al. (2013) from South
457 Korea display strong values of field intensity of 130 ZAm² at around ~1300 BCE, explained
458 either as a result of the migration of persistent flux in the northern hemisphere or as an
459 episode of geomagnetic field hemispheric asymmetry.

460 Interesting insights result from the comparison of our dataset and the data provided by
461 Mitra et al. (2013): seventeen archeointensity estimates from Senegal and Mali (West Africa)
462 covering a time period between 1000 BC and 1000 AD. These data were compared with data
463 from Morocco and Egypt, and also with European data, dividing data in three latitudinal
464 intervals: 0°-20°, 20°-40° and 40°-60° N. They found a strong latitudinal gradient in VADM
465 values, especially in the time range between 100 and 1000 AD, whereas from 0 to 1000 BC
466 both data from 20°-40° and 40°-60° reproduce a prominent feature culminating around 600
467 BC with a maximum (up to 120 ZAm²). The latitudinal gradient is explained as a changing
468 non-axial-dipole contributions and confirmed by the simulation at the core mantle boundary
469 using the Cals3k.4 model (Korte and Constable, 2011), whereas the structure of the field
470 around 0-100 AD was more axial-dipolar. Our data (at a latitude of 38°N) confirm the Mitra
471 et al. (2013) conclusion for the age interval between 400 and 1200 AD, whereas our values
472 are even higher than those in the compilation of Mitra et al. (2013), especially for the peak of
473 high intensity around 600 BC.

474

475 **6. Conclusion**

476 New paleointensity data from lava flows many of which have excellent age control from
477 the last 3,000 years (Moore 1990, 1991; and Moore and Rubin 1991) are presented in this
478 study. All the samples previously investigated to recover paleodirections have been subjected

479 to a strict pre-selection process in order to choose the most suitable samples for paleointensity
480 experiments.

481 We obtained 20 new paleointensity estimates from 13 lava flows. Ten lava flows were
482 radiocarbon dated, whereas three flows were dated archeomagnetically by Di Chiara et al.
483 (2012); one site was dated using stratigraphic relations. The archeomagnetically dated flows
484 (Cruz N, and Lagoa) have mean flow intensities that are different from those predicted and
485 we revise their ages; Cruz N is slightly older, and Lagoa could be younger or older (~1,500
486 AD or ~3,100 BC) than previously stated. The Cals10k.1b model (Korte et al. 2011) predicts
487 declinations of -3° , inclination of 52° and intensity of $39 \mu\text{T}$ around 3,400 BC. There are other
488 times when the field was low according to the model before 3,000 BC (inclination and
489 declination also), and so the dating is not certain. The age of the Cascalho flow around 1,300
490 AD is confirmed by the paleointensity.

491 The intensity of the site Sml08 assigned to the 1652 AD historical flow of Fogo 1 is
492 effectively particularly high ($78.0 \mu\text{T}$). Since the direction is also different from the expected
493 values for this age, we suggest that the flow sampled at Sml08 may be older.

494 The peak of intensity up to $\sim 90 \mu\text{T}$ around 600 BC is well supported by two sites from
495 the same flow (Furna). It is noteworthy that our results are comparable to the “spike” of
496 intensity founded West Levant records, as well as in Western Europe.

497 Our data confirm the conclusion of Mitra et al. (2013) of a predominance of the axial-
498 dipole component between 0 to 100 AD, and a strong latitudinal gradient from 100 to 1000.
499 The maximum in field values around 500-600 BC is well reproduced and even enhanced.

500 We conclude that:

501 • Archeomagnetic dating requires the three components of the geomagnetic field
502 (declination, inclination and intensity) and a well determined global model (see Lanos 2004).

503 • Since some of the studied flows diverge from the predicted paleomagnetic behavior
504 either some of earlier paper conclusions are inconsistent, or some of the flows mapped by
505 Moore (1990) may be multiple flows so the geological map needs to be improved.

506 • Our data are consistent with Mitra's et al. (2013) conclusions that there is a high field
507 gradient at 500 BC, at 0 AD, data are consistent with data and require no field gradient.
508 Around 800 AD, the gradient appears again.

509 • Our data represent the first dataset of reliable paleointensity estimates for the central-
510 northern Atlantic Ocean. The new data are internally consistent and radiocarbon dated, so
511 they can be included in global geomagnetic datasets, and safely used to enhance the next
512 global model of the geomagnetic field.

513

514

515

Acknowledgements

516 A.D.C. thanks Jason Steindorf for laboratory support, R. Mitra for useful discussions
517 and helpfulness, and acknowledges a Marco Polo grant from the Bologna University. A.D.C.
518 and F.S. were funded by INGV and FIRB MIUR C2 funds (responsible L. Sagnotti). This was
519 partially supported by National Science Foundation grant EAR1141840 to L. T.

520

521

References

522 Abdel-Monem, A.A., Fernandez, L.A., Boone, G. M., 1975. K–Ar ages from the eastern
523 Azores group (Santa Maria, São Miguel and the Formigas Islands). *Lithos.* 8(4), 247–254,
524 doi:10.1016/0024-4937(75) 90008-0.

525 Abokodair, A.A., 1977. The Accuracy of the Thelliers' Technique for the Determination
526 of Paleointensities of the Earth's Magnetic Field. PhD Thesis, University of California, Santa
527 Cruz.

528 Agostinho, J., 1937. Volcanic Activity in the Azores, Report for 1933-36: *Bulletin of*
529 *Volcanology*, 2(2), 183-92, Napoli.

530 Aitken, M. J., Allsop, A.L., Bussell, G.D., Winter, M.B., 1988. Determination of the
531 intensity of the Earth's magnetic field during archaeological times: reliability of the Thellier
532 technique. *Rev. of Geoph.* 26(1), 3-12.

533 Beamud, E., Gómez-Paccard, M., McIntosh, G., Larrasoña, J.C., 2012. New
534 archaeomagnetic data from three roman kilns in northeast Spain: a contribution to the Iberian
535 palaeosecular variation curve. *Geophysical Research Abstracts*, 14, EGU2012-8232.

- 536 Ben-Yosef, E., Tauxe, L., Levy, T.E., Shaar, R., Ron, R., Najjar, M., 2009.
537 Geomagnetic intensity spike recorded in high resolution slag deposit in Southern Jordan.
538 *Earth and Planetary Science Letters* 287, 529–539, doi:10.1016/j.epsl.2009.09.001
- 539 Ben-Yosef, E., Tauxe, L., Ron, H., Agnon, A., Avner, A., Najjar, M., Levy, T.E. 2008.
540 A new approach for geomagnetic archaeointensity research: insights on ancient metallurgy in
541 the Southern Levant. *J. Archaeol. Sci.* 35, 2863–2879.
- 542 Biggin, A.J., 2006. First-order symmetry of weak-field partial thermoremanence in
543 multi-domain (MD) ferromagnetic grains. 2. Implications for Thellier-type palaeointensity
544 determination. *Earth Planet. Sci. Lett.* 245, 454–470.
- 545 Biggin, A.J., 2010. Are systematic differences between thermal and microwave
546 Thellier-type palaeointensity estimates a consequence of multidomain bias in the thermal
547 results? *Phys. Earth Planet. Inter.* 180, 16–40.
- 548 Biggin, A.J., Poidras, T., 2006. First-order symmetry of weak-field partial
549 thermoremanence in multi-domain ferromagnetic grains. 1. Experimental evidence and
550 physical implications. *Earth Planet. Sci. Lett.* 245, 438–453.
- 551 Biggin, A.J., Thomas, D.N., 2003. Analysis of long-term variations in the geomagnetic
552 poloidal field intensity and evaluation of their relationship with global geodynamics. *Geoph.*
553 *J. Int.* 152(2), 392–415.
- 554 Booth, B., Croasdale, R., Walker, G.P.L., 1978. A quantitative study of five thousand
555 years of volcanism on São Miguel, Azores. *Philos. Trans. R. Soc. London A.* 288, 271–319,
556 doi:10.1098/rsta.1978.0018.
- 557 Bowles J., Gee J.S., Kent D., Bergmanis, E., Sinton, J., 2005. Cooling rate effects on
558 paleointensity estimates in submarine basaltic glass and implications for dating young flows.
559 *Geochem., Geophys., Geosyst.* 6, doi:10.1029/2004GC000900.
- 560 Bucur, I., 1994. The direction of the terrestrial magnetic field in France during the last
561 21 centuries. Recent progress, *Phys. Earth Planet. Inter.*, 87,95–109, doi:10.1016/0031-
562 9201(94)90024-8.
- 563 Cai, S., Tauxe, L., Deng, C., Pan, Y., Jin, G., Zheng, J., Xie, F., Qin, H., Zhu, R., (subm).
564 Geomagnetic intensity variations for the past 8 kyr: New archaeointensity results from
565 Eastern China.
- 566 Calvo, M., Prévot, M., Perrin, M., Riisager, J., 2002. Investigating the reasons for the
567 failure of palaeointensity experiments: a study on historical lava flows from Mt. Etna (Italy).
568 *Geophys. J. Int.* 149, 44–63
- 569 Carlut, J., Kent, D.V., 2000. Paleointensity record in zero-age submarine basalt glasses:
570 testing a new dating technique for recent MORBs. *Earth and Planetary Science Letters*, 183,
571 389-401.
- 572 Carlut, J., Cormier, M.H., Kent, D.V., Donnelly, K.E., Langmuir, C.H., 2004. Timing of
573 volcanism along the northern East Pacific Rise based on paleointensity experiments on
574 basaltic glasses. *J. Geophys. Res.* 109, B04104.

- 575 Carlut, J., Kent, D.V., 2002. Paleointensity record in zero-age submarine basalt glasses:
576 testing a new dating technique for recent MORBs. *Earth Planet. Sci. Lett.* 183, 389-401
- 577 Carlut, J., Quidelleur, X., Courtillot, V., Boudon, G., 2000. Paleomagnetic directions
578 and K/Ar dating of 0 to 1 Ma lava flows from La Guadeloupe Island (French West Indies):
579 Implications for time-averaged field models. *J.of Geoph. Res.* 105, 835-849.
- 580 Catanzariti, G., Gómez-Paccard, M., McIntosh, G., Pavón-Carrasco, F.J., Chauvin, A.,
581 Osete, M.L., 2012. New archaeomagnetic data recovered from the study of Roman and
582 Visigothic remains from central Spain (3rd–7th centuries). *Geophysical Journal International*,
583 doi: 10.1111/j.1365-246X.2011.05315.x.
- 584 Champion, D.E. (1980) Holocene geomagnetic secular variation in the western United
585 States : implications for the global geomagnetic field. Dissertation (Ph.D.), California
586 Institute of Technology.
- 587 Chauvin, A., Y. Garcia, Ph. Lanos, and F. Laubenheimer (2000). Paleointensity of the
588 geomagnetic field recovered on archaeomagnetic sites from France. *Physics of the Earth and
589 Planetary Interiors*, 120, 111–136.
- 590 Chauvin, A., P. Roperch, and S. Levi (2005). Reliability of geomagnetic paleointensity
591 data: the effects of the NRM fraction and concave up behaviour on paleointensity
592 determination by Thellier method, *Phys. Earth planet. Inter.*, 150, 265–286
- 593 Coe, R.S. (1967). The determination of paleo-intensities of the Earth's magnetic field
594 with emphasis on mechanisms which could cause non-ideal behavior in Thellier's method. *J.
595 Geomagn. Geoelectric.*, 19, 157-179.
- 596 Coe, R.S., Gromme, S., Manknen, E.A., 1978. Geomagnetic paleointensities from
597 radiocarbon-dated lava flows on Hawaii and the question of the Pacific nondipole low. *J.
598 Geophys. Res.* 83, 1740–1756.
- 599 Coe, R.S., Riisager, J., Plenier, G., Leonhardt, R., Kràs, D., 2004. Multidomain
600 behavior during Thellier paleointensity experiments: results from the 1915 Mt. Lassen flow.
601 *Physics of the Earth and Planetary Interiors* 147, 141–153.
- 602 Cromwell, G., Tauxe, L., Staudigel, H., Ron, H., Trusdell, F., 2011. Paleointensity
603 results for 0 and 3 ka from Hawaiian lava flows: a new approach to sampling. *American
604 Geophysical Union, Fall Meeting 2011*, abstract #GP13A-08.
- 605 Cromwell, G, Tauxe, L., Staudigel, H., Ron, H., Trusdell, F., 2012. Paleointensity
606 results for 0 and 4 ka from Hawaiiin lava flows: a new approach to sampling. *EGU General
607 Assembly, Geophysical Research Abstracts*, 14, EGU2012-01608.
- 608 Day, R., Fuller, M., Schmidt, V.A., 1977. Hysteresis properties of titanomagnetites:
609 grain-size and compositional dependence. *Physics of The Earth and Planetary Interiors* 13,
610 260–267.
- 611 De Marco, E., Spatharas, V., Gómez-Paccard, M., Chauvin, A., Kondopoulou, D., 2008.
612 New archaeointensity results from archaeological sites and variation of the geomagnetic field
613 intensity for the last 7 millennia in Greece. *Physics and Chemistry of the Earth* 33, 578–595.

- 614 Dekkers M.J., Boehnel H.N., 2006. Reliable absolute palaeointensities independent of
615 magnetic domain state. *Earth Planet. Sci. Lett.*, 248, 508-517.
- 616 Di Chiara, A., Speranza, F., Porreca, M., 2012. Paleomagnetic secular variation at the
617 Azores during the last 3 ka, *J. Geophys. Res.*, 117, B07101, doi:10.1029/2012JB009285.
- 618 Donadini, F., Korhonen, K., Riisager, P. Pesonen, L.J., 2006. Database for Holocene
619 geomagnetic intensity information, *EOS Trans. Am. Geophys. Union* 87 (14), 137.
- 620 Donadini, F., Korte, M., and Constable, C.G., 2009. Geomagnetic field for 0–3 ka: 1.
621 New data sets for global modeling, *Geochem. Geophys. Geosyst.* 10, Q06007,
622 doi:10.1029/2008GC002295.
- 623 Dunlop, D.J., 2002. Theory and application of the Day plot (Mrs/Ms versus Hcr/Hc) 1.
624 Theoretical curves and tests using titanomagnetite data, *J. Geoph. Res.* 107 (B3),
625 10.1029/2001JB000486.
- 626 Dunlop, D.J., Carter-Stiglitz, B., 2006. Day plots of mixtures of superparamagnetic,
627 single-domain, pseudosingledomain, and multidomain magnetites, *J. Geophys. Res.*, 111,
628 B12S09, doi:10.1029/2006JB004499.
- 629 Dunlop, D. J., Özdemir, Ö., 1997/2001. *Rock Magnetism, Fundamentals and Frontiers.*
630 Cambridge University Press, New York, p. 573 (paperback ed.).
- 631 Fabian, K., 2001. A theoretical treatment of paleointensity determination experiments
632 on rocks containing pseudo-single or multi domain magnetic particles. *Earth and Planetary*
633 *Science Letters* 188, 45-58.
- 634 Feraud, G., Kaneoka, I., Allègre, C.J. (1980). K/Ar ages and stress pattern in the
635 Azores: Geodynamic implications. *Earth Planet. Sci. Lett.* 46, 275–286, doi:10.1016/0012-
636 821X(80)90013-8.
- 637 Ferk A., Leonardht, R., Richard, D., Aulock, F., Hess, K., Dingwell, D., 2008.
638 Paleointensity study on subaerial volcanic glass. *Geophysical Research Abstracts*, Vol. 10,
639 EGU2008-A-06936.
- 640 Gallet, Y., Le Goff, M., 2006. High-temperature archeointensity measurements from
641 Mesopotamia. *Earth Planet. Sci. Lett.*, 241, 159–173.
- 642 Gallet, Y., Genevey, A., Le Goff, M., 2002. Three millennia of directional variation of
643 the Earth's magnetic field in western Europe as revealed by archaeological artefacts, *Phys.*
644 *Earth Planet. Inter.*, 131, 81–89, doi:10.1016/S0031-9201(02)00030-4.
- 645 Gallet, Y., Genevey, A., Courtillot, V., 2003. On the possible occurrence of
646 archeomagnetic jerks in the geomagnetic field over the past three millennia. *Earth and*
647 *Planetary Science Letters* 214, 237–242.
- 648 Gallet, Y., Genevey, A., Le Goff, M., Fluteau, F., Eshraghi, S.A., 2006. Possible impact
649 of the Earth's magnetic field on the history of ancient civilizations. *Earth Planet. Sci. Lett.*,
650 246, 17– 26.
- 651 Garcia, A.S., Thomas, D.N., Liss, D., Shaw, J., 2006. Low geomagnetic field intensity
652 during the Kiaman superchron: Thellier and microwave results from the Great Whin Sill

- 653 intrusive complex, northern United Kingdom. *Geophysical Research Letters* 33(16), doi:
654 10.1029/2006GL026729.
- 655 Gee, J.S., Cande, S.C., Hildebrand, J.A., Donnelly, K., Parker, R.L., 2000. Geomagnetic
656 intensity variations over the past 780 kyr obtained from near-seafloor magnetic anomalies.
657 *Nature* 408, 827–832.
- 658 Genevey, A., Gallet, Y., 2002. Intensity of the geomagnetic field in western Europe over
659 the past 2000 years: new data from ancient French potteries. *J. Geophys. Res.* 107,
660 doi:10.1029/2001JB000701.
- 661 Genevey, A., Gallet, Y., Rosen, J., Le Goff, M., 2009. Evidence for rapid geomagnetic
662 field intensity variations in Western Europe over the past 800 years from new French
663 archaeointensity data. *Earth and Plan. Sci. Lett.* 284, 132–143.
- 664 Genevey, A., Gallet, Y., Margueron, J.-C., 2003. Eight thousand years of geomagnetic
665 field intensity variations in the eastern Mediterranean. *Journal of Geophysical Research* 108,
666 doi: 10.1029/2001JB001612.
- 667 Genevey, A., Gallet, Y., Rosen, J., Le Goff, M., 2009. Evidence for rapid geomagnetic
668 field intensity variations in Western Europe over the past 800 years from new French
669 archaeointensity data. *Earth and Plan. Sci. Lett.* 284, 132–143.
- 670 Genevey, A., Gallet, Y., Constable, C.G., Korte, M., Hulot, G., 2008. ArcheoInt: An
671 upgraded compilation of geomagnetic field intensity data for the past ten millennia and its
672 application to the recovery of the past dipole moment. *Geochem. Geophys. Geosyst.* 9(4),
673 Q04038, doi:10.1029/2007GC001881.
- 674 Gómez-Paccard, M., Chauvin, A., Lanos, P., Thiriot, J., 2008. New archeointensity data
675 from Spain and the geomagnetic dipole moment in western Europe over the past 2000 years.
676 *J. Geophys. Res.* 113, B09103, doi:10.1029/2008JB005582.
- 677 Gómez-Paccard, M., Chauvin, A., Lanos, P., McIntosh, G., Osete, M.L., Catanzariti, G.,
678 Ruiz-Martínez, V.C., Núñez, J.I., 2006. First archaeomagnetic secular variation curve for the
679 Iberian Peninsula: Comparison with other data from western Europe and with global
680 geomagnetic field models. *Geochem. Geophys. Geosyst.* 7, Q12001,
681 doi:10.1029/2006GC001476.
- 682 Gómez-Paccard, M., McIntosh, G., Chauvin, A., Beamud, E., Pavón-Carrasco, F.J.,
683 Thiriot, J., 2012. Archaeomagnetic and rock magnetic study of six kilns from North Africa
684 (Tunisia and Morocco). *Geophys. J. Int.* 189, 169–186. doi: 10.1111/j.1365-
685 246X.2011.05335.x.
- 686 Granot, R., Tauxe, L., Gee, J.S., Ron, H., 2006. A view into the Cretaceous
687 geomagnetic field from analysis of gabbros and submarine glasses. *Earth and Planetary
688 Science Letters* 256(1-2), 1-11.
- 689 Gubbins, D., Jones, A.L., Finlay, C.C., 2006. Fall in Earth's Magnetic Field Is Erratic.
690 *Science* 312, 900–902.
- 691 Hagstrum, J.T., Champion, D.E., 1994. Paleomagnetic correlation of Late Quaternary
692 lava flows in the lowest east rift zone of Kilauea Volcano, Hawaii. *J. Geophys. Res.* 99 (B11),
693 21679-21690.

- 694 Hartmann, G.A., Trindade, R.I.F., Goguitchaichvili, A., Etchevarne, C., Morales, J.,
695 aAfonso, M.C., 2009. First archeointensity results from Portuguese potteries (1550–1750
696 AD). *Earth Planets Space*, 61, 93–100.
- 697 Herrero-Bervera, E., Valet, J.P., 2009. Testing determinations of absolute paleointensity
698 from the 1955 and 1960 Hawaiian flows. *Earth and Planetary Science Letters* 287, 420–433.
- 699 Hill, M. J., Shaw, J., 2000. Magnetic field intensity study of the 1960 Kilauea lava flow,
700 Hawaii, using the microwave palaeointensity technique. *Geophys. J. Int.*, 142, 487–504.
- 701 Hill, M.J., Gratton, M.N., Shaw, J., 2002. A comparison of thermal and microwave
702 palaeomagnetic techniques using lava containing laboratory induced remanence. *Geophys. J.*
703 *Int.* 151, 157–163.
- 704 Hoffman, K.A., Constantine, V.L., Morse, D.L., 1989. Determination of absolute
705 paleointensity using a multi-specimen procedure. *Nature* 339, 295–297.
- 706 Hong, H., Yu, Y., Hee Lee, C., Kim, R.H., Park, J., Doh, S.J., Kim, W., Sung, J., 2013.
707 Globally strong geomagnetic field intensity circa 3000 years ago. *Earth and Planetary Science*
708 *Letters*, 383, 142–152.
- 709 Jackson, A., Jonkers, A.R.T., Walker, M. R., 2000. Four centuries of geomagnetic
710 secular variation from historical records. *Royal Society of London Philosophical*
711 *Transactions*, 358, 957-990.
- 712 Johnson, C. L., Wijbrans, J.R., Constable, C.G., Gee, J., Staudigel, H., Tauxe, L.,
713 Forjaz, V.H., Salgueiro, M., 1998. $^{40}\text{Ar}/^{39}\text{Ar}$ ages and paleomagnetism of São Miguel lavas,
714 Azores. *Earth and Planetary Science Letters* 160, 637–649.
- 715 Kissel, C., Laj, C., 2004. Improvements in procedure and paleointensity selection
716 criteria (PICRIT-03) for Thellier and Thellier determinations: application to Hawaiian basaltic
717 long cores. *Physics of the Earth and Planetary Interiors* 147, 155–169.
- 718 Kletetschka, G., Fuller, M.D., Kohout, T., Wasilewski, P.J., Herrero-Bervera, E., Ness,
719 N.F., Acuna, M.H., 2006. TRM in low magnetic fields: a minimum field that can be recorded
720 by large multi domain grains. *Phys. Earth Planet. Inter.* 154, 290–298.
- 721 Korte, M., Constable, C.G., 2011. Improving geomagnetic field reconstruction for 0–3
722 ka, *Phys. Earth Planet. Inter.* 188, 247–259, doi:10.1016/j.pepi.2011.06.017.
- 723 Korte, M., Donadini, F., Constable, C.G., 2009. Geomagnetic field for 0 – 3 ka: 2. A
724 new series of time-varying global models. *Geochem. Geophys. Geosyst.*, 10, Q06008,
725 doi:10.1029/2008GC002297.
- 726 Korte, M., Constable, C.G., Donadini, F., Holme, R., 2011. Reconstructing the
727 Holocene geomagnetic field: *Earth and Planetary Science Letters* 312(3–4), 497–505.
- 728 Kovacheva, M., 1984. Some archaeomagnetic conclusions from three archaeological
729 localities in North-West Africa. *Comptes Rendus de l'Acad. Bulgare des Sci.* 3712, 171-174.
- 730 Lanos, P., 2004. Bayesian inference of calibration curves: application to
731 archaeomagnetism. In: Buck, C., Millard, A. (Eds.), *Tools for Constructing Chronologies:*
732 *Crossing Disciplinary Boundaries.* Springer-Verlag, London 177, 43-82.

- 733 Leonhardt, R., Krása, D., and Coe, R.S., 2004. Multidomain behavior during Thellier
734 paleointensity experiments: a phenomenological model *Physics of the Earth and Planetary*
735 *Interiors* 147, 127–140.
- 736 Levi, S., 1977. The effect of Magnetite particle size on paleointensity determinations of
737 the geomagnetic field. *Physics of the Earth and Planetary Interiors* 13, 245-259.
- 738 McClelland, E., Briden, J.C., 1996. An improved methodology for Thellier-type
739 paleointensity determination in igneous rocks and its usefulness for verifying primary
740 thermoremanence. *J. Geophys. Res.* 101, 21995–22013.
- 741 Merrill, R.T., McElhinny, M.W., Mc Fadden, P.L., 1996). The Magnetic field of the
742 Earth, Paleomagnetism, the Core, and Deep Mantle. International geophysics series, Vol 63.
- 743 Michalk, D.M., Muxworthy, A.R., Böhnell, H.N., MacLennan, J., Nowaczyk, J.N. 2008.
744 Evaluation of the multispecimen parallel differential pTRM method: a test on historical lavas
745 from Iceland and Mexico. *Geophys. J. Int.* 173, 409–420.
- 746 Mitchell-Thomè, R.C., 1981. Vulcanicity of historic times in the Middle Atlantic
747 Islands, *Bull. Volcanol.*, 44, 57–69.
- 748 Mitra, R., Tauxe, L., and Mcintosh, S.K., 2013. Two thousand years of archeointensity
749 from West Africa. *Earth and Planetary Science Letters*, 364, 123–133
- 750 Moore, R.B., 1990. Volcanic geology and eruption frequency, São Miguel, Azores,
751 *Bull. Volcanol.*, 52, 602–614, doi:10.1007/BF00301211.
- 752 Moore, R.B., 1991. Geologic map of São Miguel, Azores, U.S. Geol. Surv. Misc.
753 Invest. Map, I-2007, scale 1:50,000.
- 754 Moore, R.B., Rubin, M., 1991. Radiocarbon dates for lava flows and pyroclastic
755 deposits on São Miguel, Azores, *Radiocarbon*, 33(1), 151–164.
- 756 Nachasova, I.E., Burakov, K.S., Molina, F., Cámara, J.A., 2007. Archaeomagnetic
757 study of ceramics from the Neolithic Los Castillejos multilayer monument (Montefrio,
758 Spain), *Izvestiya, Physics of the Solid Earth* 43(2), 170-176.
- 759 Nachasova, I. E., Burakov, K.S., 2009. Variation of the intensity of the Earth's
760 magnetic field in Portugal in the 1st Millennium BC. *Physics of the Solid Earth* 45(7), 595–
761 603.
- 762 Nagata, T., Arai, Y., Momose, K., 1963. Secular variation of the geomagnetic total
763 force during the last 5000 years. *J. Geophys. Res.* 68, 5277–5281.
- 764 Pan, Y., Shaw, J., Zhu, R., Hill, M.J., 2002. Experimental reassessment of the Shaw
765 paleointensity method using laboratory-induced thermal remanent magnetization. *Journal of*
766 *Geophysical Research* 107, B7, doi:10.1029/2001JB000620, 2002.
- 767 Paterson, G.A., 2010. Decisions, decisions: The selection of paleointensity data.
768 American Geophysical Union, Fall Meeting 2011, abstract #GP13A-08.

- 769 Paterson, G.A., Biggin, A.J., Yamamoto, Y., Pan, Y., 2012. Towards the robust
770 selection of Thellier-type paleointensity data: The influence of experimental noise. *Geoch.*
771 *Geoph. Geosyst.* 13(5), Q05Z43, doi:10.1029/2012GC004046.
- 772 Pick, T., Tauxe, L., 1993. Geomagnetic palaeointensities during the Cretaceous normal
773 superchron measured using submarine volcanic glass. *Nature* 366, 238–242.
- 774 Pressling, N., Laj, C., Kissel, C., Champion, D., Gubbins, D., 2006. Palaeomagnetic
775 intensities from ¹⁴C-dated lava flows on the Big Island, Hawaii: 0–21 kyr. *Earth and*
776 *Planetary Science Letters* 247, 26–40.
- 777 Pressling, N., Brown, M.C., Gratton, M.N., Shaw, J., Gubbins, D., 2007. Microwave
778 palaeointensities from Holocene age Hawaiian lavas: Investigation of magnetic properties and
779 comparison with thermal palaeointensities. *Physics of the Earth and Planetary Interiors* 162,
780 99–118.
- 781 Pressling, N., Trusdell, F.A., Gubbins, D., 2009. New and revised ¹⁴C dates for
782 Hawaiian surface lava flows: Paleomagnetic and geomagnetic implications. *Geophys. Res.*
783 *Lett.* 36, L11306, doi:10.1029/2009GL037792.
- 784 Riisager, P., Riisager, J., 2001. Detecting multidomain magnetic grains in Thellier
785 palaeointensity experiments. *Physics of the Earth and Planetary Interiors* 125, 111–117.
- 786 Schweitzer, C., Soffel, H.C., 1980. Paleointensity measurements on postglacial lavas
787 from Iceland. *J. Geophys.* 47, 57–60.
- 788 Selkin, P.A., Tauxe, L., 2000. Long-term variations in palaeointensity. *Philosophical*
789 *Transactions of the Royal Society of London A* 358, 1065–1088.
- 790 Shaar, R., Tauxe, L., 2013. Thellier GUI: An integrated tool for analyzing
791 paleointensity data from Thellier-type experiments, *Geochem. Geophys. Geosyst.* 14, 677–
792 692, doi:10.1002/ggge.20062.
- 793 Shaar, R., Ron, H., Tauxe, L., Kessel, R., Agnon, A., 2011. Paleomagnetic field
794 intensity derived from non-SD: Testing the Thellier IZZI technique on MD slag and a new
795 bootstrap procedure. *Earth and Planetary Science Letters* 310, 213–224.
- 796 Shaw, J., Walton, D., Ang, S., Rolph, T.C., Share, J.A., 1996. Microwave
797 archaeointensity from Peruvian ceramics. *Geophys. J. Int.* 124, 241–244.
- 798 Shaw, J., 1974. A new method of determining the magnitude of the palaeomagnetic
799 field, application to five historic lavas and five archaeological samples. *Geophys. J. R. Astron.*
800 *Soc.*, 39, 133–141.
- 801 Sherwood, G.J. 1991. Evaluation of a multi-specimen approach to paleointensity
802 determination. *J. Geomag. Geoelectr.* 43, 341–349.
- 803 Smirnov, A.V., Tarduno, J.A., Pisakin, B.N., 2003. Paleointensity of the early
804 geodynamo (2.45 Ga) as recorded in Karelia: A single-crystal approach. *Geology* 31, 415–
805 418.

806 Stanton, T., Riisager, P., Knudsen, M.F., Thørdarson, T., 2011. New paleointensity data
807 from Holocene Icelandic lavas. *Phys. Earth Planet. Inter.* 186 (1–2), 1–10,
808 doi:10.1016/j.pepi.2011.01.006.

809 Stuiver, M., Reimer, P.J., Reimer, R.W., 2009. CALIB 6.0 program and documentation:
810 <http://calib.qub.ac.uk/calib> (March 2012).

811 Tanaka, H., Kono, M., 1991. Preliminary results and reliability of palaeointensity
812 studies on historical and ¹⁴C dated Hawaiian lavas. *J. Geomagn. Geoelect.* 43, 375–388.

813 Tanaka H., Hashimoto, Y., Morita, N., 2012. Palaeointensity determinations from
814 historical and Holocene basalt lavas in Iceland. *Geophys. J. Int.* 189, 833–845 doi:
815 10.1111/j.1365-246X.2012.05412.x.

816 Tanaka, H., Kono, M., Kaneko, S., 1995. Paleosecular variation of direction and
817 intensity from two Pliocene-Pleistocene lava sections in Southwestern Iceland. *J. Geomag.*
818 *Geoelectr.* 47, 89–102.

819 Tarduno, J. A., Cottrell, R. D., Smirnov, A.V., 2001. High geomagnetic field intensity
820 during the mid-Cretaceous from Thellier analyses of single plagioclase crystals. *Science* 291,
821 1779-1783.

822 Tauxe, L., 2009. *Essentials of Paleomagnetism*, University of California Press,
823 Berkeley.

824 Tauxe, L., Mullender, T.A.T., Pick, T., 1996. Potbellies, waspwaists, and
825 superparamagnetism in magnetic hysteresis. *Geophys. Res.* 101, 571 – 583.

826 Tauxe, L., Staudigel, H., 2004. Strength of the geomagnetic field in the Cretaceous
827 Normal Superchron: New data from submarine basaltic glass of the Troodos Ophiolite.
828 *Geoch. Geoph. Geosyst.* 5(5), Q02H06. doi:10.1029/2003GC000635.

829 Tauxe, L., Yamazaki, T., 2007. Paleointensities, in *Treatise on Geophysics*, edited by
830 M. Kono. *Treatise on Geophysics* 5, 509– 563, Elsevier, New York.

831 Tauxe, L., Bertram, N.H., Seberino, C., 2002. Physical interpretation of hysteresis
832 loops: Micromagnetic modeling of fine particle magnetite. *Geoch. Geoph. Geosyst.* 3(10),
833 doi:10.1029/2001GC000241.

834 Tema, E., D. Kondopoulou, 2011. Secular variation of the Earth's magnetic field in the
835 Balkan region during the last eight millennia based on archaeomagnetic data. *Geophys. J. Int.*
836 186, 603–614.

837 Tema, E., J. Morales, A. Goguitchaichvili, P. Camps, 2013. New archaeointensity data
838 from Italy and geomagnetic field intensity variation in the Italian Peninsula. *Geophys. J. Int.*
839 193,603–614.

840 Thellier, E., Thellier, O., 1959. Sur l'intensité du champ magnétique terrestre dans le
841 passé historique et géologique. *Annales de Géophysique* 15, 285–376.

842 Thomas, D.N., Hill, M., Garcia, A.S., 2004. Comparison of the Coe–Thellier–Thellier
843 and microwave palaeointensity techniques using high-titanium titanomagnetites: results from

844 a Tertiary basaltic intrusion from the Sydney Basin, New South Wales. *Earth Planet. Sci.Lett.*
845 229, 15– 29.

846 Tsunakawa, H., Shaw, J., 1994. The Shaw method of paleointensity determinations and
847 its application to recent volcanic rocks. *Geophys. J. Int.* 118, 781–787.

848 Valet, J. P., Herrero-Barvera, E., 2000. Paleointensity experiments using alternating
849 field demagnetization. *Earth Planet. Sci.Lett.* 177, 43-58.

850 Valet, J.P., Herrero-Bervera, E., Carlut, J., Kondopoulou, D., 2010. A selective
851 procedure for absolute paleointensity in lava flows. *Geophys. Res. Lett.* 37, L16308,
852 doi:10.1029/2010GL044100.

853 Van der Geer, J., Hanraads, J.A.J., Lupton, R.A., 2010. The art of writing a scientific
854 article. *J. Sci. Commun.* 163, 51–59.

855 Xu, S., Dunlop, D.J., 1995. Theory of partial thermoremanent magnetization in
856 multidomain grains. 2. Effect of microcoercivity distribution and comparison with
857 experiment. *J. Geophys. Res.* 99, 9025–9033.

858 Xu, S., Dunlop, D.J., 2004. Thellier paleointensity theory and experiments for
859 multidomain grains. *J. Geophys. Res.* 109, B07103. doi:10.1029/2004JB003024.

860 Yamamoto, Y., Tsunakawa, H., Shibuya, H., 2003. Palaeointensity study of the 1960
861 Hawaiian lava: implications for possible causes of erroneously high intensities. *Geophys. J.*
862 *Int.* 153, 263–276.

863 Yu, Y., Tauxe., L., 2005. Testing the IZZI protocol of geomagnetic field intensity
864 determination. *Geoch. Geoph. Geosyst.* 6 (5), Q05H17, doi: 10.1029/2004GC000840.

865 Yu, Y., Tauxe, L., Genevey, A., 2004. Toward an optimal geomagnetic field intensity
866 determination technique. *Geoch. Geoph. Geosyst.* 5 (2), Q02H07, doi:
867 10.1029/2003GC000630.

868

869

870 **Figure captions**

871 Fig.1. Location of sampling sites of studied flows in Sao Miguel (Azores Archipelago,
872 Portugal) showed in the Digital Elevation Model. The “Sml” prefix of each site is omitted.
873 Flow geometry, characteristics, and ages are after Moore (1990, 1991). 1563 and 1652 AD
874 flows are historic. Calendar ages of the other lava flows were calibrated by us using
875 CALIB6.0 (<http://calib.qub.ac.uk/calib/calib.html>) from original ¹⁴C ages reported by Moore
876 and Rubin (1991). Flow ages indicated with parentheses were paleomagnetically inferred (Di
877 Chiara et al., 2012). Grey symbols of paleomagnetic sites indicate that all the samples from
878 site were rejected from paleointensity analyses. The inset represents the geomagnetic field

879 “flux patches”, arising from the non-axial dipole component. There are two of these positive
880 anomalies in the northern hemisphere, one over Eurasia and one over North America.

881

882 Fig. 2 a) Day plot (Day et al., 1977). SD, PSD, and MD refer to Single, Pseudo-single,
883 and Multi domain behavior. The red line represent the theoretical mixing SD MD equations
884 of Dunlop (2002) using the constraints of Dunlop and Carter-Stiglitz (2006).

885 Fig. 3 Representative IZZI and hysteresis experimental results. a-c) Hysteresis loops at
886 1T of sister specimens from three samples. d-f) Fractional magnetization versus temperature
887 of all the samples of the flows Mos, Furna, and Feteiras. g-i) Arai plots and insets of
888 Zijderveld diagrams of the specimens. The temperature interval used for isolating the
889 characteristic remanence is marked with green line and squares. The insets are the vector
890 components of the zero field steps with x in the abscissa and y and z in the ordinate. The
891 circles are (x, y) pairs and the squares (the temperature steps are marked alongside) are (x, z)
892 pairs. The directions are in the specimen coordinate system. The laboratory field was of 40
893 μT , applied along the z-axis in the in-field steps.

894 Fig. 4 a) Declination and b) inclination of paleomagnetic directions previously recovered by
895 Di Chiara et al. (2012), versus age plot for historical and ^{14}C dated site mean directions. In a)
896 and b) declination /inclination are compared with global field model prediction from gufm1
897 (Jackson et al., 2000) CALS3k.4 (Korte and Constable, 2011), ARCH3k.1 (Korte et al., 2009)
898 and the French curve (Bucur 1994, Gallet et al., 2002). c) Paleointensity results (this study)
899 from all specimen (blue dots) and mean intensities obtained from each flow. Ages are
900 calendar ages calibrated from ^{14}C ages reported by Moore and Rubin (1991) using CALIB6.0
901 (<http://calib.qub.ac.uk/calib/calib.html>).

902 Fig. 5 Paleointensity flow means are compared with data from Morocco (Gomez-Paccard et
903 al., 2012) and Europe: Portugal (Nachasova and Bukarov 2009; and Hartmann et al., 2009;),
904 Spain (Gomez-Paccard et al., 2006; 2008; 2012; Nachasova et al., 2006; Catanzariti et al.,
905 2012; Beamud et al., 2012), and France (Chauvin et al., 2000; Genevey and Gallet 2002;
906 Gallet et al., 2003; 2009; Genevey et al., 2009; Gomez-Paccard et al., 2012).

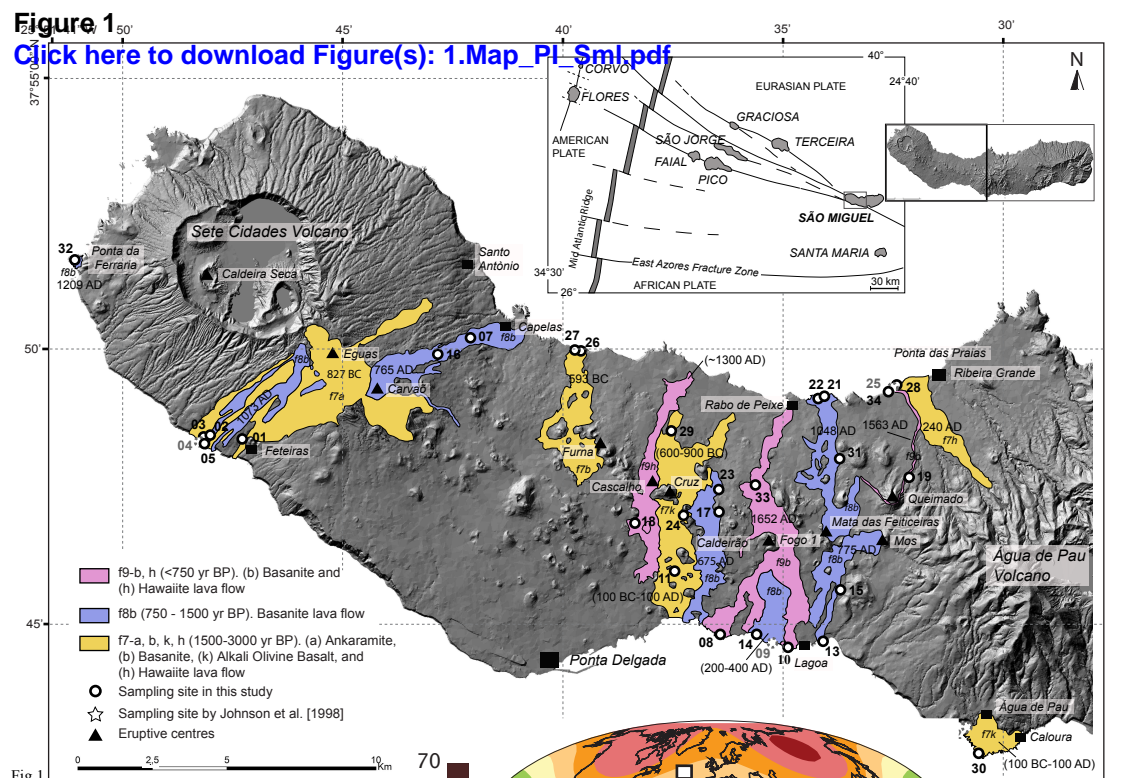


Figure 2

[Click here to download Figure\(s\): 2_Dayplot_Pi_Sml.pdf](#)

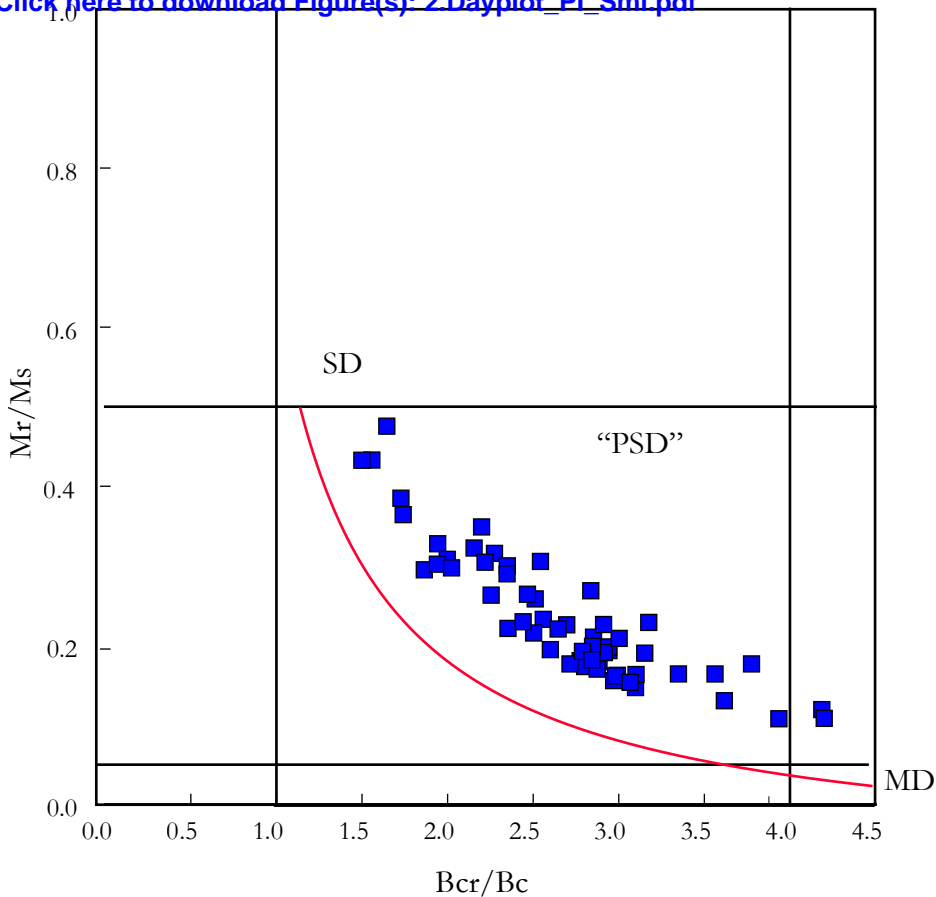


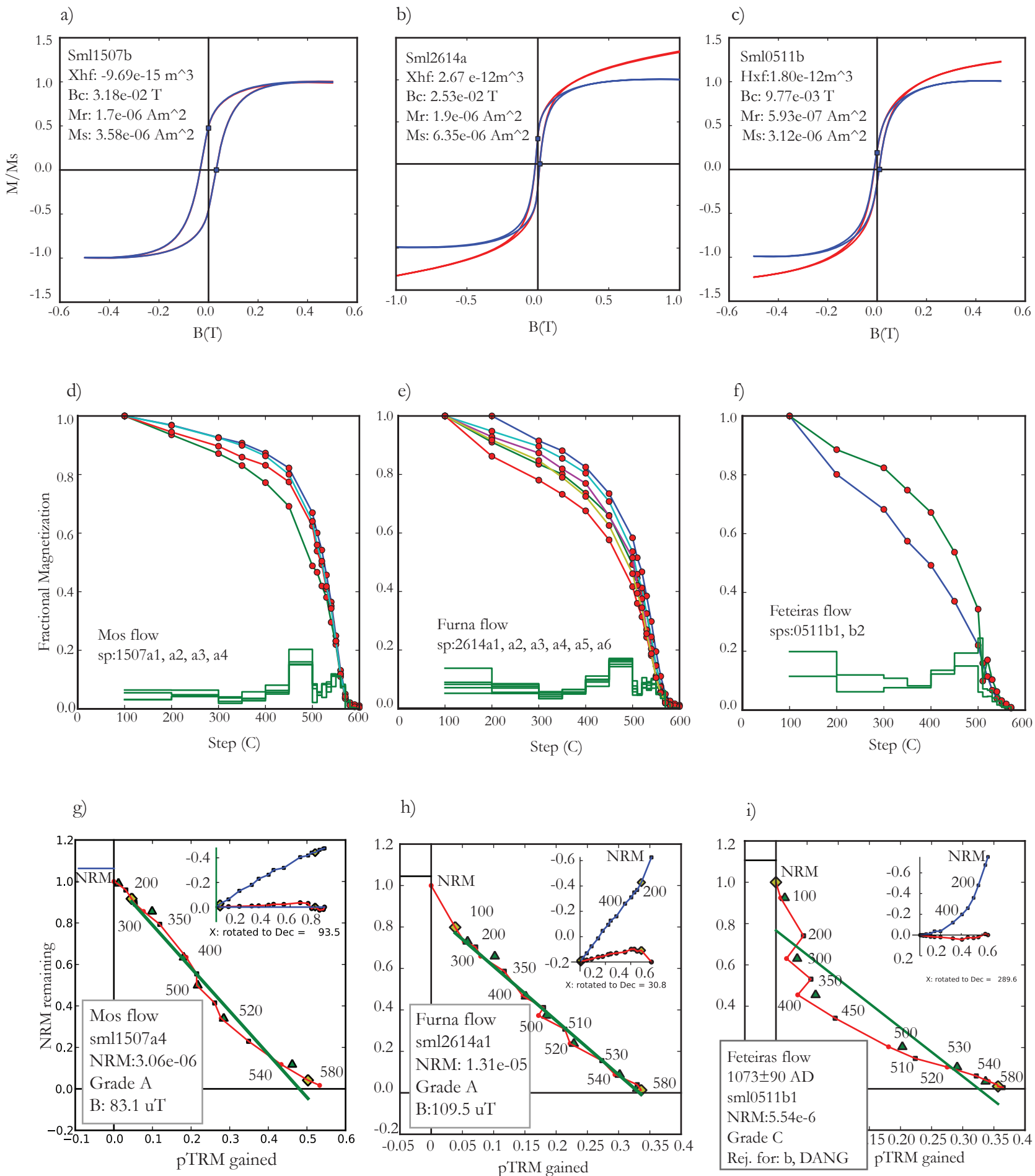
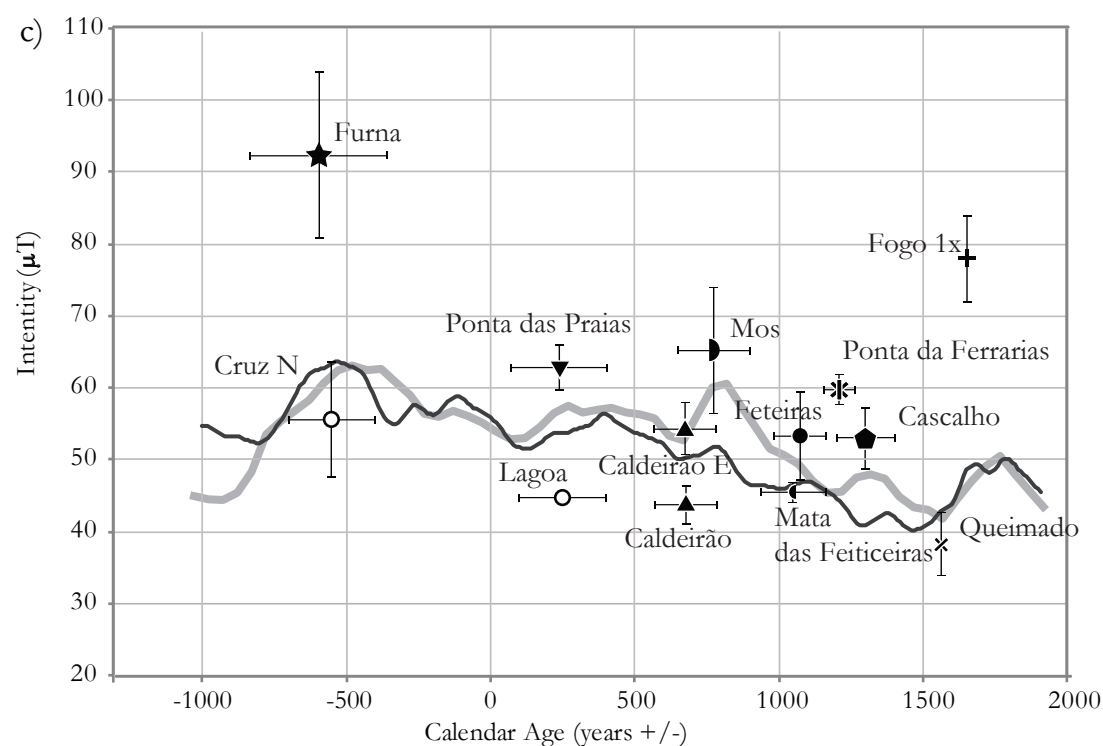
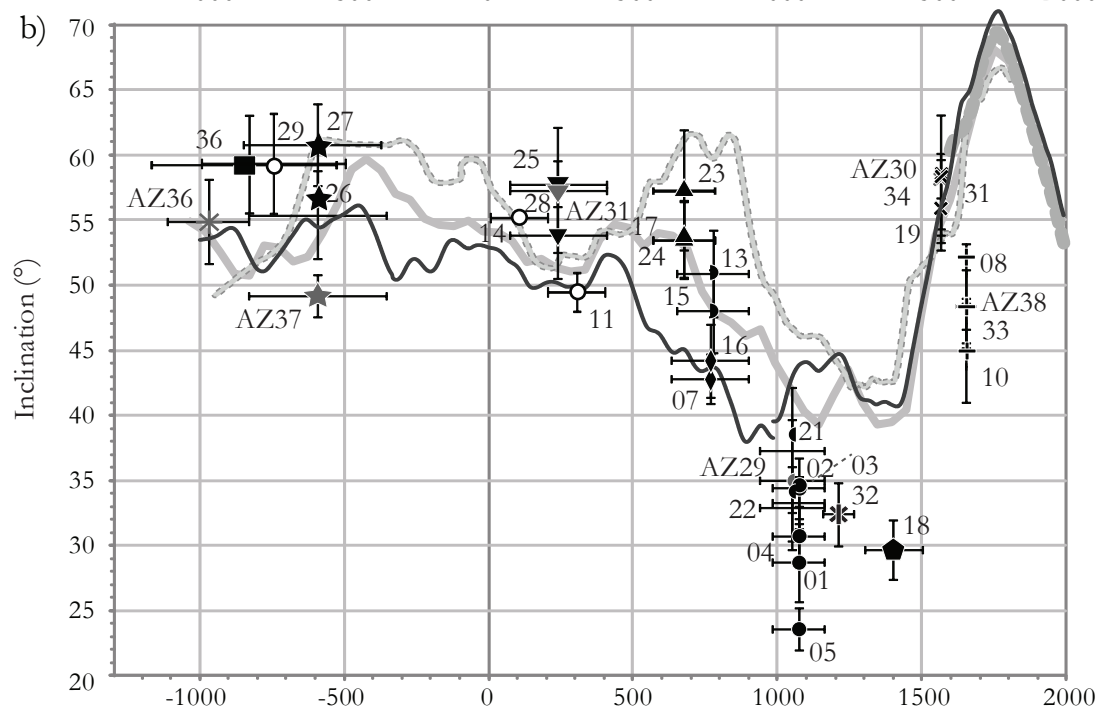
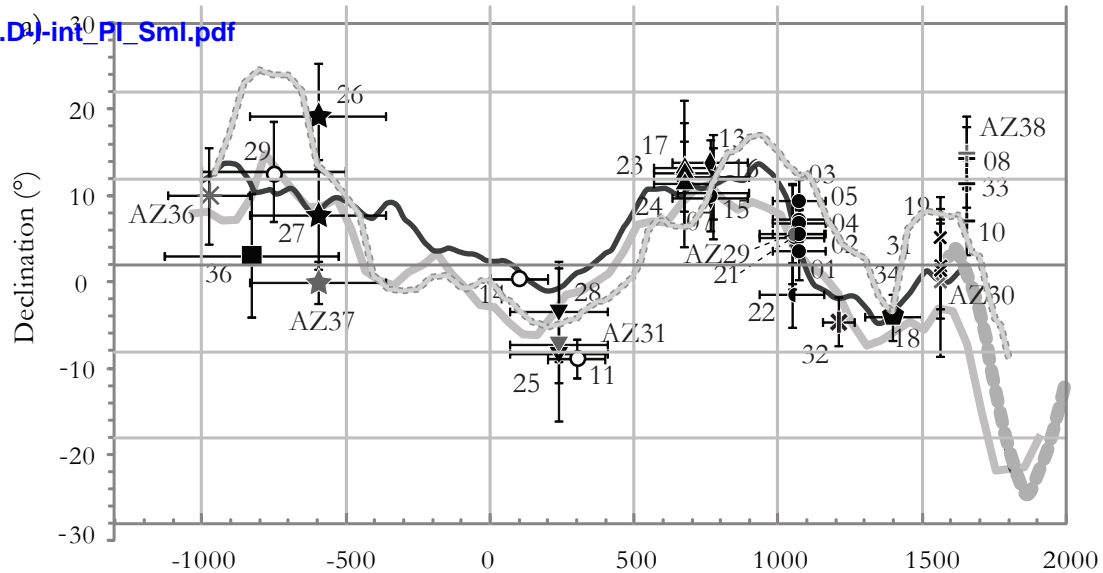
Figure 3[Click here to download Figure\(s\): 3.Zijd-dmag-araiplot_PI_Sml.pdf](#)

Figure 4

[Click here to download Figure\(s\): 4.Da-int_PI_Sml.pdf](#)

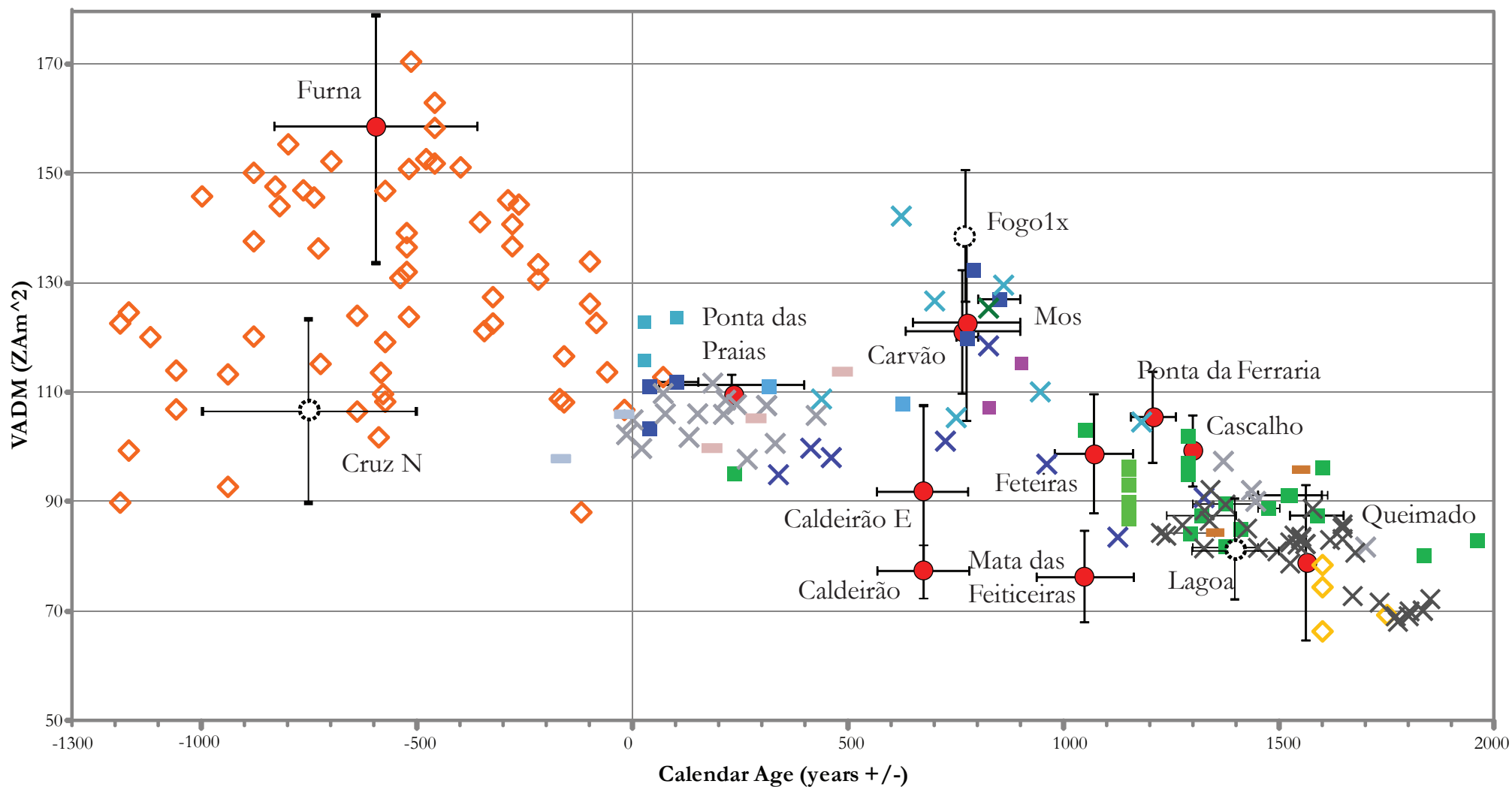


Sampled sites:

- ✚ Fogo (1652 AD)
- ✕ Queimado (1563 AD)
- ⬢ Cascalho (1300 AD)
- ✱ Ponta da Ferraria (1209±54 AD)
- Feteiras (1073±90 AD)
- ◐ Mata das Feiticeiras (1048±113 AD)
- ◑ Mos (775±124 AD)
- ◆ Carvão (765±132 AD)
- ▲ Caldeirão (675±107 AD)
- ▼ Ponta das Praias (240±168 AD)
- ★ Furna (593±236 BC)
- Eguas (827±305 BC)
- Site mean with age interferred
- AZ- Sites by Johnson et al. [1998]
- Sample mean intensity (this study)

PSVcurves:

- CALS3K.4 (Korte and Constable, 2011)
- gufm1 (Jackson et al. 2000)
- - - PSV France (Bucur, 1994 and Gallet et al., 2002)
- Arch3k.1 (Korte et al., 2009)

Figure 5[Click here to download Figure\(s\): 5.data_comparison_PI_Sml.pdf](#)

- | | | |
|--------------------------------------|---------------------------------------|---------------------------------------|
| ● Intensity (this study) | ■ Spain (Catanzariti et al., 2012) | ✕ France (Genevey and Gallet 2002) |
| ⊗ Intensity inferred (this study) | ■ Spain (Beaumod et al., 2012) | ✕ France (Gallet et al., 2009) |
| ■ Spain (Gomez-Paccard et al., 2006) | ◇ Portugal (Nachasova et al., 2009) | ✕ France (Genevey et al., 2009) |
| ■ Spain (Nachasova et al., 2007) | ◇ Portugal (Hartmann et al., 2009) | ■ Morocco (Kovacheva 1984) |
| ■ Spain (Gomez-Paccard et al., 2008) | ✕ France (Chauvin et al., 2000) | ■ Morocco (Gomez-Pacard et al., 2012) |
| ■ Spain (Gomez Paccard et al., 2012) | ✕ France (Gomez Paccard et al., 2012) | ■ Morocco (Gomez-Pacard et al., 2012) |

Table1 - Location of sampling sites at São Miguel

Flow name	Site	Lat (N)	Lon (W)	Age Uncalibrated (years BP)	Age (years±AD)
Furna	Sml26	37.832	25.661	2460±220	593±236 BC
	Sml27	37.832	25.659		
Cruz N	Sml29	37.807	25.626	1500–3000	400-700 BC*
Caloura	Sml30	37.708	25.511	1500–3000	0-200 AD*
Cruz S	Sml11	37.764	25.620		0-200 AD*
Lagoa	Sml14	37.744	25.594	750–1500	100-400 AD*
Ponta das Praias	Sml28	37.819	25.540	1790±150 AD	240±168 AD
	Sml25	37.819	25.540		
Caldeirão	Sml17	37.782	25.608	1350±120 AD	675±107 AD
Caldeirão E	Sml23	37.789	25.609		
Caldeirão W	Sml24	37.780	25.621		
Carvão	Sml07	37.835	25.702	1280±150 AD	765±132 AD
	Sml16	37.829	25.714		
Mos	Sml13	37.742	25.569	1250 ±150 AD	775±124 AD
	Sml15	37.758	25.561		
Mata das Feiticeiras	Sml21	37.817	25.567	1010 ±120 AD	1048±113 AD
	Sml22	37.816	25.569		
Feteiras	Sml01	37.801	25.801		1073 ±90 AD
	Sml02	37.801	25.801		
	Sml03	37.804	25.804		
	Sml05	37.803	25.803		
Cascalho	Sml18	37.779	25.643	Less than 500±100and 663± 105 AD	1300±100 AD**
Ponta da Ferraria	Sml32	37.861	25.854	840 ±60 AD	1209±53 AD
Queimado	Sml19	37.792	25.535		1563 AD
	Sml31	37.798	25.562		
	Sml34	37.818	25.542		
Fogo 1	Sml10	37.740	25.582		1652 AD
	Sml33	37.790	25.594		
Fogo 1X	Sml08	37.740	25.608		

Site coordinates were gathered by a Garmin GPS using WGS84 datum. Units and uncalibrated ^{14}C ages with an error of 1s are from Moore [1990, 1991] and Moore and Rubin [1991]. *Flows whose age is defined by an age interval. **Flows whose age was paleomagnetic dated by Di Chiara et al. [2012]. Calendar ages were calibrated using the Stuiver's program CALIB6.0 Online [<http://calib.qub.ac.uk>]

Table 2 - Threshold values of quality criteria

Sample criteria			Specimen criteria						
N	σ (%)	σ (μ T)	N	β	DANG	SCAT	FRAC	int _{mad}	N _{ptm}
3	15	5	3	0.1	10	True	0.85	10	2

Quality parameters: n is the minimum number of samples or specimen, beta is a scatter parameter, DRATS is the Difference of the RATio Sum [Tauxe and Staudiguel, 2004]

Table 3

Table 3 - Paleointensity results from sites and flows from São Miguel

Flow name	Sites	Age (year+/-)	σ (Age)	Dec (°)	Inc (°)	α_{95}	Intensity					
							N_B	B (μ T)	σ	σ (%)	VADM	σ_{VADM}
Furna	Sml26;27	-593	236	13.0	58.0	2.7	17	92.3	11.6	12.5	163.5	20.5
Cruz N	Sml29	-750	250	8.7	57.5	2.6	7	55.7	8	14.3	98.8	14.1
Lagoa	Sml14	300	100	1.0	54.3	4.1	4	44.9	1.1	2.3	79.6	1.9
Ponta das Praias	Sml28	240	168	356.0	56.0	2.0	4	63.0	3.2	5.0	111.6	5.6
Caldeirão	Sml17	675	107	(-)	(-)	(-)	4	44.1	0.9	1.9	78.2	1.5
Caldeirão E	Sml23	675	107	12.6	57.3	4.6	3	54.5	3.5	6.5	96.6	6.3
Mos	Sml13;15	775	124	10.2	48.5	2.3	13	65.2	8.8	13.4	115.8	15.5
Mata das Feiticeiras	Sml21	1048	113	1.1	34.2	2.5	6	45.7	1.4	3.1	81.0	2.5
Feteiras	Sml01;02;03;05	1073	90	6.4	32.7	1.1	11	53.5	6.1	11.4	94.8	10.8
Ponta da Ferraria	Sml32	1209	54	355.4	32.4	2.4	5	60.0	2.1	3.5	106.2	3.7
Cascalho	Sml18	1300	0	355.9	29.7	2.3	7	53.1	4.2	7.9	94.2	7.4
Queimado	Sml19;31;34	1563	0	0.5	55.5	1.5	11	38.5	4.3	11.1	68.2	7.6
Fogo 1x	Sml08	1652	0	11.1	47.7	2.3	8	78.0	5.9	7.6	138.4	10.5

Flow names and ages are defined as in Table 1. Age in bold are questioned in this study. Ages in italic character are age intervals "paleomagnetically inferred" after Di Chiara et al. [2012]. Declination and Inclination are from previous study. N is the number of specimens. Mean intensity results are reported by flow (μ T and VADM converted), after IZZI experiments and processed using the pmagpy-2.214 by L. Tauxe.

Supplementary Material

[Click here to download Supplementary Material: S1.Arai plots-zijd.pdf](#)

Supplementary Material

[Click here to download Supplementary Material: S2.pdf](#)